PRG 006 ©July 2014

QUEEN'S UNIVERSITY

POLYMERS RESEARCH GROUP

19 Division Street, Kingston, ON, K7L 3N6 Canada

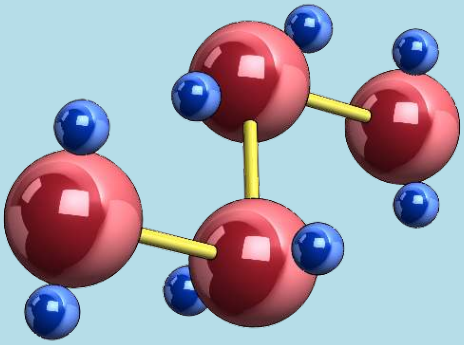

LARGE-AMPLITUDE OSCILLATORY SHEAR: COMPARING PARALLEL-DISK WITH CONE-PLATE FLOW

A.J. Giacomin[1,*], P.H. Gilbert[1], D. Merger[2] and M. Wilhelm[2]

[1]Chemical Engineering Department
Polymers Research Group
Queen's University
Kingston, ON K7L 3N6

[2]Karlsruhe Institute of Technology
Institut fuer Technische und Polymerchemie
1876128 Karlsruhe, Germany

*Corresponding author (giacomin@queensu.ca)

QU-CHEE-PRG-TR--2014-6

LARGE-AMPLITUDE OSCILLATORY SHEAR: COMPARING PARALLEL-DISK WITH CONE-PLATE FLOW

A.J. Giacomin[1,*], P.H. Gilbert[1], D. Merger[2] and M. Wilhelm[2]

[1]Chemical Engineering Department
Polymers Research Group
Queen's University
Kingston, ON K7L 3N6

[2]Karlsruhe Institute of Technology
Institut fuer Technische und Polymerchemie
1876128 Karlsruhe, Germany

ABSTRACT

We compare the ratio of the amplitudes of the third to the first harmonic *of the torque*, $|\mathscr{T}_3|/|\mathscr{T}_1|$, measured in rotational parallel-disk flow, with the ratio of the corresponding harmonics *of the shear stress*, $|\tau_3|/|\tau_1|$, that would be observed in sliding-plate or cone-plate flow. In other words, we seek a *correction factor* with which $|\mathscr{T}_3|/|\mathscr{T}_1|$ must be multiplied, to get the quantity $|\tau_3|/|\tau_1|$, where $|\tau_3|/|\tau_1|$ is obtained from any simple shearing flow geometry. In this paper, we explore theoretically, the disagreement between $|\mathscr{T}_3|/|\mathscr{T}_1|$ and τ_3/τ_1 using the simplest continuum model relevant to large-amplitude oscillatory shear flow: the single relaxation time corotational Maxwell model. We focus on the region where the harmonic amplitudes and thus, their ratios, can be fully described with power laws. This gives the expression for $|\mathscr{T}_3|/|\mathscr{T}_1|$, by integrating the explicit analytical solution for the shear stress. In the power law region, we find that, for low Weissenberg numbers, for the third harmonics $|\mathscr{T}_3|/|\mathscr{T}_1| = \frac{2}{3}|\tau_3|/|\tau_1|$, and for the fifth harmonics, $|\mathscr{T}_5|/|\mathscr{T}_1| = \frac{1}{2}|\tau_5|/|\tau_1|$. We verify these results experimentally. In other words, the heterogeneous flow field of the parallel-disk geometry significantly attenuates the higher harmonics, when compared with the homogeneous, sliding-plate flow. This is because only the outermost part of the sample is subject to the high shear rate amplitude. Further, our expression for the torque in large-amplitude oscillatory parallel-disk flow is also useful for the simplest design of viscous torsional dampers, that is, those incorporating a viscoelastic liquid between two disks.

* Corresponding author (giacomin@queensu.ca).

CONTENTS

TABLES

FIGURES

I. INTRODUCTION

Since its conception in 1935 [1], oscillatory shear flow has become the most common way of measuring viscoelastic properties, and of late, this same test, performed at large-amplitude has sustained growing popularity [2]. This test can be used to differentiate materials by amplifying subtle differences in small-amplitude oscillatory shear behavior [3]. It has thus been used to elucidate problems in plastics processing, such as shaping in blow molding, for example [4]. Sometimes, parallel-disk flow is chosen for oscillatory shear flow measurements, and in particular, for large-amplitude oscillatory shear flow. By *parallel-disk flow*, we mean the flow generated between two parallel disks, when one disk rotates relative to the other (see Figure **1**). About the choice of parallel-disk flow for large-amplitude oscillatory shear, Stickel et al. [5] write "with few exceptions, the linear mappings between torque and stress (at the rim) and between displacement and strain are still commonly employed with LAOS rheometry, despite the ample literature describing nonlinear material responses to LAOS." In this work, we consider the measurement of viscoelastic properties, at large shear rate amplitudes, using oscillatory shear flow.

The sources of error for torsional flow form a subset of those in cone-plate flow. However, secondary flows are not promoted by the presence of normal stress differences in this case (see Section 5.3 of [6]). Also, for the cone-plate geometry, positioning the cone can take a long time. This is why parallel-disk flow is often chosen over cone-plate flow, for oscillatory shear measurement. The parallel-disk geometry is also advantageous for suspensions of particles or fibers [7], since, for cone-plate flow, the particle size can approach the gap near the cone apex (or near the cone tip truncation). Thus, for some materials, cone-plate flow cannot be used at all, and thus, for large-amplitude oscillatory shear, one must resort to parallel-disk flow [8,9].

When fluid inertia can be neglected [10,11,12], the resulting flow field is given by [13,14]:

$$v_x = \dot{\gamma}^0 \cos\omega t\, y;\; v_y = v_z = 0 \tag{1}$$

where the shear rate amplitude, $\dot{\gamma}^0$, is the product of the *shear strain amplitude* and the angular frequency, ω. The flow given by In Eq. (1) can either be generated between sliding-plates (or for a close approximation, between a shallow cone and a plate [see caption to Figure 1]). This sliding-plate flow for oscillatory shear is illustrated in Figure 2, which, along with **Table I**, defines the Cartesian coordinates. The shear rate corresponding to Eq. (1) may then be written as:

$$\lambda\dot{\gamma}(t) = \lambda\dot{\gamma}^0 \cos\lambda\omega(t/\lambda) \tag{2}$$

in which the dimensionless shear rate $\lambda\dot{\gamma}^0$ (the Weissenberg number), the dimensionless frequency $\lambda\omega$ (the Deborah number), appear [15], and where λ is any characteristic time for the fluid.

Unlike sliding-plate flow (or its close approximant cone-plate flow) whose flow fields are homogeneous (see in Figure 2), parallel-disk flow is a heterogeneous flow field (see Figure 1) given by:

$$v_\theta = \Omega^0 r\left(z/h\right)\cos\omega t; v_z = v_r = 0 \tag{3}$$

so that the shear rate is given by:

$$\dot{\gamma}_{r\theta} = \dot{\gamma}_R^0\left(r/R\right)\cos\omega t \tag{4}$$

and thus, its amplitude is proportional to radial position (and thus the distance from the center) in cylindrical coordinates (defined in Figure 3 along with **Table I**). Eq. (4) can be nondimensionalized as:

$$\lambda\dot{\gamma}_{r\theta} = \lambda\dot{\gamma}_R^0\left(r/R\right)\cos\lambda\omega\left(t/\lambda\right) \tag{5}$$

and, in general, when using parallel-disk flow for oscillatory shear, we identify $\lambda\dot{\gamma}_R^0$ in Eq. (4) with $\lambda\dot{\gamma}^0$ in Eq. (2).

Since large-amplitude oscillatory shear properties are themselves strain-rate amplitude dependent, the heterogeneity of the parallel-disk flow field complicates the interpretation of the measured torque. To see why, we first consider the connection between the torque and the shear stress in the parallel-disk fixture for any fluid, and specifically, the torque that the fluid exerts on the stationary plate (see EXAMPLE 10.1-2 in [16]):

$$\begin{aligned}\mathscr{T} &= -\int_0^{2\pi}\int_0^R r\tau_{\theta z}\cdot r\,dr\,d\theta \\ &= -2\pi\int_0^R r^2\tau_{\theta z}\,dr\end{aligned} \tag{6}$$

from which, it has been shown that (see Eqs. (5a) and (5b) of [17]; see also Eq. (5) of [18]; [19]; see Eq. (10) and Fig. 2 of the Supplemental Information [20] to [21]):

$$\tau_{r\theta} = \frac{1}{2\pi R^3}\left(\theta_0\frac{d\mathscr{T}}{d\theta_0} + 3\mathscr{T}\right) \tag{7}$$

Eqs. (6) and (7) are deduced from the equations of motion, and thus apply to all fluids. Thus, getting $\tau_{r\theta}$ requires an accurate determination of $d\mathscr{T}/d\theta_0$, and this at least involves numerical differentiation that can amplify noise (see how to cope with this in [22]; see also APPENDIX IV of [23] or the EXPERIMENTAL section of [24]). The use of Eq. (7) for extracting higher harmonics of the shear stress response large-amplitude oscillatory shear flow from the observed torque in parallel-disk flow, have been reported ([25], see also Figs. 1 and 2 of [17]; Fig. 3 of [18]).

For a fixed test frequency, Eq. (7) requires that we take the derivative of every Fourier component of the torque with respect to the strain rate amplitude at the rim. Thus, torque measurements with high signal-to-noise ratios [26,27], and many experiments at different strain rate amplitude at the rim, are required. For polymer solutions, shear strain amplitudes up to $\dot{\gamma}^0/\omega = 27$ are reported. Measurements at much lower values of $\dot{\gamma}^0/\omega$ have been corroborated with cone-plate flow data. These methods are tedious, but they involve no constitutive

assumptions. In fact, one reason that experimentalists would prefer parallel-disks for oscillatory shear, is that the edge distortions arising in rotational rheometry are postponed to much larger values of $\dot{\gamma}^0/\omega$ than for cone-plate flow. For an iconic photograph of these edge distortions in parallel-disk flow, see Fig. 2. of [28]. Another reason that the parallel-disk geometry is often preferred over cone-plate, is that it takes far less time for the insertion normal thrust to vanish after sample loading.

Less general schemes to extract non-sinusoidal large-amplitude oscillatory properties from parallel-disk flow experiments have been developed [5,29,30,31], but these assume specific constitutive relations to relate the measured torque to the shear stress. Since a single constitutive equation will not be valid for all fluids, the more general approach of MacSporran and Spiers [25] seems preferable, if parallel-disk flow is to be used.

In this paper, we focus particularly on the ratio of the amplitudes of harmonics (third-to-first and fifth-to-first), often called the *relative intensities,* a now widely established way of representing large-amplitude oscillatory shear measurements (see Fig. 2 of [32]; see Fig. 4.12 of [33,34]; see Fig. 6 of [35]). This concept of relative intensities follows naturally from the analysis of molecular spectroscopy [33], and has become a popular way of summarizing nonlinear viscoelastic behavior. Additionally, it allows for spectral averaging to substantially increase the signal-to-noise ratio [26]. The symbol $I_{3/1}$ is often used for the amplitude ratio, $|\tau_3|/|\tau_1|$, and:

$$\lim_{\left(\dot{\gamma}^0/\omega\right)\to 0} \frac{|\tau_3|/|\tau_1|}{\left(\dot{\gamma}^0/\omega\right)^2} \equiv Q_0^{3/1} \tag{8}$$

where $\left(\dot{\gamma}^0/\omega\right)$ is the shear strain amplitude. $Q_0^{3/1}$ has been named the *intrinsic nonlinearity* (for a thorough treatment of this quantity see [36]). We recognize that $I_{3/1}$, has been used interchangeably for both $|\mathscr{T}_3|/|\mathscr{T}_1|$ and $|\tau_3|/|\tau_1|$, regardless of the geometry. However, since this paper is specifically about the ratio of $|\mathscr{T}_3|/|\mathscr{T}_1|$ to $|\tau_3|/|\tau_1|$, we use $I_{3/1}$ strictly to mean $|\tau_3|/|\tau_1|$ measured in the cone-plate or sliding plate fixture. This limit is inspired by the usual expansions for the steady shear viscosity, or for the shear stress response in large-amplitude oscillatory shear, which give generally (see Eqs. (147) and (157) of [15]; see Eq. (3) of [32]; [37,38,39]):

$$|\tau_h|/|\tau_1| \propto \left(\dot{\gamma}^0/\omega\right)^{h-1}; h>1, \text{odd} \tag{9}$$

and specifically:

$$|\tau_3|/|\tau_1| \propto \left(\dot{\gamma}^0/\omega\right)^2 \tag{10}$$

where h is the integer number of the harmonic.

Wagner et al. [40] have shown that for fluids with shear stress responses conforming to the expansion in odd powers of $\dot{\gamma}_0/\omega$ (Eq. (147) of [15]):

$$\frac{\tau_{yx}(t)}{\gamma_0} = -\sum_{\substack{m=1 \\ \text{odd}}}^{\infty} \sum_{\substack{n-1 \\ \text{odd}}}^{m} \gamma_0^{m-1} \left[G'_{mn}(\omega) \sin n\tau + G''_{mn}(\omega) \cos n\tau \right] \tag{11}$$

which defines a set of pairs of nonlinear moduli (see Table I), Wagner et al. [40] get, for $\dot{\gamma}^0/\omega$ small enough for the harmonic amplitudes and thus, their ratios, to be fully described with power laws (see Eq. (37) of [40]:

$$\frac{|\tau_h|/|\tau_1|}{|\mathscr{T}_h|/|\mathscr{T}_1|} = \frac{3+h}{4} \tag{12}$$

They use the factor given by Eq. (12) with $h = 3$ to correct the third-to-first torque amplitude ratio measured in parallel-disk flow. For instance, $\frac{3}{2}|\mathscr{T}_3|/|\mathscr{T}_1|$ is used as an estimate of $|\tau_3|/|\tau_1|$, and $2|\mathscr{T}_5|/|\mathscr{T}_1|$ is used as an estimate of $|\tau_5|/|\tau_1|$. We find that analytical solutions to constitutive equations only occasionally come out in the form of Eq. (11) [28,40,41]. Instead, more commonly (see column "Notation Eq." of Table 1 of [15]), they come out as odd powers of $\dot{\gamma}^0$, defining a matrix of frequency dependent nonlinear viscosities ([42]; Eq. (157) of [15]), and which defines a set of pairs of nonlinear viscosities (see Table I):

$$\frac{\tau_{yx}(t)}{\dot{\gamma}_0} = -\sum_{\substack{n=1 \\ \text{odd}}}^{\infty} \sum_{\substack{m=1 \\ \text{odd}}}^{n} \dot{\gamma}^{0\,n-1} \left[\eta'_{mn}(\omega) \cos m\tau + \eta''_{mn}(\omega) \sin m\tau \right] \tag{13}$$

as does the corotational Maxwell model that we use herein [Eq. (19)]. By *corotational* Maxwell, we mean that the derivative in the Maxwell model (formally defined in Eq. (15) below) measures a time rate of change of the extra stress tensor with respect to a coordinate system that translates and rotates with the fluid, but does not also deform with the fluid. This corotating frame distinguishes the model from codeformational Maxwell models, where a different derivative is used that measures this rate of change with respect to a coordinate system that translates, rotates and also deforms with the fluid. When the corotational derivative is replaced with a codeformational one, all higher harmonics disappear. This is why codeformational models are not helpful for describing large-amplitude oscillatory shear flow behavior.

The corotational Maxwell model is (with tensor-valued quantities in **bold**):

$$\boldsymbol{\tau} + \lambda \frac{\mathscr{D}\boldsymbol{\tau}}{\mathscr{D}t} = -\eta_0 \dot{\boldsymbol{\gamma}} \tag{14}$$

in which:

$$\frac{\mathscr{D}\boldsymbol{\tau}}{\mathscr{D}t} \equiv \frac{D\boldsymbol{\tau}}{Dt} + \tfrac{1}{2}\{\boldsymbol{\omega}\cdot\boldsymbol{\tau} - \boldsymbol{\tau}\cdot\boldsymbol{\omega}\} \tag{15}$$

defines the corotational derivative (also called the Jaumann derivative); here $D\boldsymbol{\tau}/Dt$ is the substantial derivative of $\boldsymbol{\tau}$ (see Section 3.5 of [43]) where:

$$\frac{D}{Dt} \equiv \frac{d}{dt} + \mathbf{v}\cdot\nabla \tag{16}$$

and:

$$\dot{\boldsymbol{\gamma}} = \nabla\mathbf{v} + (\nabla\mathbf{v})^{\dagger} \tag{17}$$

is the rate-of-strain tensor, and:

$$\boldsymbol{\omega} = \nabla\mathbf{v} - (\nabla\mathbf{v})^{\dagger} \tag{18}$$

is the vorticity tensor. For a detailed treatment of the corotational Maxwell model see Chapters 7 and 8 of [44], and for its evaluation in large-amplitude oscillatory shear, see [15]. The corotational Maxwell model can also be used to explore complex flows arising in plastics processing, both analytically [44,45,46,47,48,49,50], and numerically [51,52].

II. ANALYSIS

If (see [23,24,53,54,55,56,57]) and when (see Section 6 of [15] for a detailed analysis of startup of large-amplitude oscillatory shear flow) the shear stress response to large-amplitude oscillatory shear flow reaches *alternance* (cycle-to-cycle periodicity [15] and thus, time-steady in the frequency domain), for the corotational Maxwell fluid (from Eq. (58) of [15,58]):

$$\tau_{\theta z} = \frac{\eta_0}{\lambda}\left[\begin{array}{l} -\left(\lambda\dot{\gamma}^0\right)\dfrac{\cos\tau + \lambda\omega\sin\tau}{1+L} \\ \quad + \dfrac{\left(\lambda\dot{\gamma}^0\right)^3}{4}\left[\begin{array}{l} \dfrac{3\cos\tau + 6\lambda\omega\sin\tau}{(1+L)(1+4L)} \\ + \dfrac{(1-11\mathrm{L})\cos 3\tau + 6(1-L)\lambda\omega\sin 3\tau}{(1+L)(1+4L)(1+9L)} \end{array}\right] \\ -\dfrac{\left(\lambda\dot{\gamma}^0\right)^5}{8}\left[\begin{array}{l} \dfrac{5\cos\tau + 15\lambda\omega\sin\tau}{(1+L)(1+4L)(1+9L)} \\ + \left[\dfrac{(5-130L)\cos 3\tau + (45-120L)\lambda\omega\sin 3\tau}{2(1+L)(1+4L)(1+9L)(1+16L)}\right] \\ + \left[\dfrac{\left(1-85L+274L^2\right)\cos 5\tau + \left(15-225L+120L^2\right)\lambda\omega\sin 5\tau}{2(1+L)(1+4L)(1+9L)(1+16L)(1+25L)}\right] \end{array}\right] \\ +\cdots \end{array}\right] \tag{19}$$

where $L \equiv \lambda^2\omega^2$ and $\tau \equiv \omega t$, and which has general form:

$$\tau = \sum_{\substack{n=1 \\ \text{odd}}}^{\infty}\sum_{\substack{h=0 \\ \text{odd}}}^{n}\tau_{h,n} = \tau_{1,1} + \left[\tau_{1,3} + \tau_{3,3}\right] + \left[\tau_{1,5} + \tau_{3,5} + \tau_{5,5}\right] + \cdots \tag{20}$$

where the brackets group nonlinear terms of equal n, $\tau_{h,n}$ are contributions from the term in the nth order of $\left(\lambda\dot{\gamma}^0\right)$ to the hth harmonic of the shear stress. This clarifies how FT-rheology and linear oscillatory rheology correspond. Thus, FT-rheology is the natural extension of linear oscillatory rheology.

For parallel-disk flow, where the shear rate amplitude is proportional to the radial position, measured with cylindrical coordinates centered on and between the parallel-disks:

$$\lambda\dot{\gamma}^0 = \lambda\dot{\gamma}^0_R\left(\frac{r}{R}\right) \tag{21}$$

Substituting Eq. (21) into Eq. (19), and then the result into Eq. (6) yields:

$$\mathscr{T} = \sum_{\substack{n=1\\ \text{odd}}}^{\infty}\sum_{\substack{h=0\\ \text{odd}}}^{n}\mathscr{T}_{h,n} = \mathscr{T}_{1,1} + \left[\mathscr{T}_{1,3} + \mathscr{T}_{3,3}\right] + \left[\mathscr{T}_{1,5} + \mathscr{T}_{3,5} + \mathscr{T}_{5,5}\right] + \cdots \tag{22}$$

where the brackets group nonlinear terms of equal n, $\mathscr{T}_{h,n}$ are contributions from the term in the nth order of $\left(\lambda\dot{\gamma}^0\right)$ in Eq. (19) to the hth harmonic of the torque, and these contributions are given by:

$$\mathscr{T}_{1,1} = 2\pi\frac{\eta_0}{\lambda}\frac{\cos\tau+\lambda\omega\sin\tau}{1+L}\lambda\dot{\gamma}^0_R\frac{1}{R}\int_0^R r^3\,dr \tag{23}$$
$$= \frac{\pi}{2}\frac{\eta_0}{\lambda}\frac{\cos\tau+\lambda\omega\sin\tau}{1+L}\left(\lambda\dot{\gamma}^0_R\right)R^3$$

$$\mathscr{T}_{1,3} = -2\pi\frac{\eta_0}{\lambda}\frac{\left(\lambda\dot{\gamma}^0_R\right)^3}{4}\left[\frac{3\cos\tau+6\lambda\omega\sin\tau}{(1+L)(1+4L)}\right]\frac{1}{R^3}\int_0^R r^5\,dr \tag{24}$$
$$= -\frac{\pi}{2}\frac{\eta_0}{\lambda}\left(\lambda\dot{\gamma}^0_R\right)^3\left[\frac{3\cos\tau+6\lambda\omega\sin\tau}{(1+L)(1+4L)}\right]\frac{R^3}{6}$$

$$\mathscr{T}_{3,3} = -\frac{\pi}{2}\frac{\eta_0}{\lambda}\left(\lambda\dot{\gamma}^0_R\right)^3\left[\frac{(1-11\mathrm{L})\cos3\tau+6(1-L)\lambda\omega\sin3\tau}{(1+L)(1+4L)(1+9L)}\right]\frac{1}{R^3}\int_0^R r^5\,dr \tag{25}$$
$$= -\frac{\pi}{2}\frac{\eta_0}{\lambda}\left(\lambda\dot{\gamma}^0_R\right)^3\left[\frac{(1-11\mathrm{L})\cos3\tau+6(1-L)\lambda\omega\sin3\tau}{(1+L)(1+4L)(1+9L)}\right]\frac{R^3}{6}$$

$$\mathscr{T}_{1,5} = \frac{\pi}{4}\frac{\eta_0}{\lambda}\left[\frac{5\cos\tau+15\mathrm{De}\sin\tau}{\left(1+\mathrm{De}^2\right)\left(1+4\mathrm{De}^2\right)\left(1+9\mathrm{De}^2\right)}\right]\left(\lambda\dot{\gamma}^0_R\right)^5\frac{1}{R^5}\int_0^R r^7\,dr \tag{26}$$
$$= \frac{\pi}{4}\frac{\eta_0}{\lambda}\left(\lambda\dot{\gamma}^0_R\right)^5\left[\frac{5\cos\tau+15\mathrm{De}\sin\tau}{\left(1+\mathrm{De}^2\right)\left(1+4\mathrm{De}^2\right)\left(1+9\mathrm{De}^2\right)}\right]\frac{R^3}{8}$$

$$\mathscr{T}_{3,5} = \frac{\pi}{4}\frac{\eta_0}{\lambda}\left(\lambda\dot{\gamma}^0_R\right)^5\left[\frac{(5-130L)\cos3\tau+(45-120L)\lambda\omega\sin3\tau}{2(1+L)(1+4L)(1+9L)(1+16L)}\right]\frac{1}{R^5}\int_0^R r^7\,dr \tag{27}$$
$$= \frac{\pi}{4}\frac{\eta_0}{\lambda}\left(\lambda\dot{\gamma}^0_R\right)^5\left[\frac{(5-130L)\cos3\tau+(45-120L)\lambda\omega\sin3\tau}{2(1+L)(1+4L)(1+9L)(1+16L)}\right]\frac{R^3}{8}$$

$$\mathscr{T}_{5,5} = \frac{\pi}{4}\frac{\eta_0}{\lambda}\left(\lambda\dot{\gamma}^0_R\right)^5\left[\frac{\left(1-85L+274L^2\right)\cos5\tau+\left(15-225L+120L^2\right)\lambda\omega\sin5\tau}{2(1+L)(1+4L)(1+9L)(1+16L)(1+25L)}\right]\frac{1}{R^5}\int_0^R r^7\,dr \tag{28}$$
$$= \frac{\pi}{4}\frac{\eta_0}{\lambda}\left(\lambda\dot{\gamma}^0_R\right)^5\left[\frac{\left(1-85L+274L^2\right)\cos5\tau+\left(15-225L+120L^2\right)\lambda\omega\sin5\tau}{2(1+L)(1+4L)(1+9L)(1+16L)(1+25L)}\right]\frac{R^3}{8}$$

By substituting Eq. (21) into Eq. (19), and then the result into Eq. (6), we are choosing a simpler path than solving the problem from scratch in cylindrical coordinates, as has been outlined for steady parallel-disk flow (see Problem **7C.4** of [44]).

III. ANALYTICAL RESULTS

In the following sections, we will use Eq. (19), and Eqs. (22) through (28) to determine successively the total torque, the amplitudes of the first, third and fifth harmonics of the total torque, the amplitudes of the corresponding harmonics of the shear stress, and finally, the corrections needed to go from torque ratios of the harmonics from parallel-disk measurements, to their corresponding shear stress amplitude harmonic ratios. Our analysis proceeds for a single characteristic time for the fluid, λ, but we discuss the case of multiple relaxation times near the end of Section III. h.

a. Total Torque

For oscillatory parallel-disk flow, substituting Eqs. (23) through (28) into Eq. (22) gives:

$$\mathscr{T} = \frac{\pi}{2}\frac{\eta_0}{\lambda}R^3\left\{\begin{array}{l} -\left(\lambda\dot{\gamma}_R^0\right)\left[\dfrac{\cos\tau+\lambda\omega\sin\tau}{1+L}\right] \\ +\dfrac{\left(\lambda\dot{\gamma}_R^0\right)^3}{6}\left[\left[\dfrac{3\cos\tau+6\lambda\omega\sin\tau}{(1+L)(1+4L)}\right]\right. \\ \qquad \left.+\left[\dfrac{(1-11\mathrm{L})\cos3\tau+6(1-L)\lambda\omega\sin3\tau}{(1+L)(1+4L)(1+9L)}\right]\right] \\ -\dfrac{\left(\lambda\dot{\gamma}_R^0\right)^5}{16}\left[\left[\dfrac{5\cos\tau+15\lambda\omega\sin\tau}{(1+L)(1+4L)(1+9L)}\right]\right. \\ \qquad +\left[\dfrac{(5-130L)\cos3\tau+(45-120L)\lambda\omega\sin3\tau}{2(1+L)(1+4L)(1+9L)(1+16L)}\right] \\ \qquad \left.+\left[\dfrac{\left(1-85L+274L^2\right)\cos5\tau+\left(15-225L+120L^2\right)\lambda\omega\sin5\tau}{2(1+L)(1+4L)(1+9L)(1+16L)(1+25L)}\right]\right] \\ +\cdots \end{array}\right\} \tag{29}$$

which happens to be the working equation for the simplest design of a torsional viscous damper (employing a viscoelastic liquid between two disks).

b. Torque Harmonics

Thus, the hth harmonics of the torque $\mathscr{T}_h$ are given by:

$$\mathscr{T}_1 = \frac{\pi}{2}\frac{\eta_0}{\lambda}R^3\left\{\begin{array}{l} -\left(\lambda\dot{\gamma}_R^0\right)\left[\dfrac{\cos\tau+\lambda\omega\sin\tau}{1+L}\right] \\ +\dfrac{\left(\lambda\dot{\gamma}_R^0\right)^3}{6}\left[\dfrac{3\cos\tau+6\lambda\omega\sin\tau}{(1+L)(1+4L)}\right] \\ -\dfrac{\left(\lambda\dot{\gamma}_R^0\right)^5}{16}\left[\dfrac{5\cos\tau+15\lambda\omega\sin\tau}{(1+L)(1+4L)(1+9L)}\right] \\ +\cdots \end{array}\right\} \tag{30}$$

$$\mathscr{T}_3 = \frac{\pi}{2}\frac{\eta_0}{\lambda}R^3\left\{\begin{array}{l} \dfrac{\left(\lambda\dot{\gamma}_R^0\right)^3}{6}\left[\dfrac{(1-11\mathrm{L})\cos3\tau+6(1-L)\lambda\omega\sin3\tau}{(1+L)(1+4L)(1+9L)}\right] \\ -\dfrac{\left(\lambda\dot{\gamma}_R^0\right)^5}{16}\left[\dfrac{(5-130L)\cos3\tau+(45-120L)\lambda\omega\sin3\tau}{2(1+L)(1+4L)(1+9L)(1+16L)}\right] \\ +\cdots \end{array}\right\} \tag{31}$$

$$\mathscr{T}_5 = \frac{\pi}{2}\frac{\eta_0}{\lambda}R^3\left\{\begin{array}{l} -\dfrac{\left(\lambda\dot{\gamma}_R^0\right)^5}{16}\left[\dfrac{\left(1-85L+274L^2\right)\cos5\tau+\left(15-225L+120L^2\right)\lambda\omega\sin5\tau}{2(1+L)(1+4L)(1+9L)(1+16L)(1+25L)}\right] \\ +\cdots \end{array}\right\} \tag{32}$$

c. Torque Harmonic Amplitudes

The amplitudes of these torque harmonics are thus given by:

$$\left|\mathscr{T}_1\right| = \frac{\pi}{2}\frac{\eta_0}{\lambda}R^3\sqrt{\left\{\begin{array}{l} -\left(\lambda\dot{\gamma}_R^0\right)\left[\dfrac{1}{1+L}\right] \\ +\dfrac{\left(\lambda\dot{\gamma}_R^0\right)^3}{6}\left[\dfrac{3}{(1+L)(1+4L)}\right] \\ -\dfrac{\left(\lambda\dot{\gamma}_R^0\right)^5}{16}\left[\dfrac{5}{(1+L)(1+4L)(1+9L)}\right] \\ +\cdots \end{array}\right\}^2 + \left\{\begin{array}{l} -\left(\lambda\dot{\gamma}_R^0\right)\left[\dfrac{\lambda\omega}{1+L}\right] \\ +\dfrac{\left(\lambda\dot{\gamma}_R^0\right)^3}{6}\left[\dfrac{6\lambda\omega}{(1+L)(1+4L)}\right] \\ -\dfrac{\left(\lambda\dot{\gamma}_R^0\right)^5}{16}\left[\dfrac{15\lambda\omega}{(1+L)(1+4L)(1+9L)}\right] \\ +\cdots \end{array}\right\}^2} \tag{33}$$

$$\left|\mathscr{T}_3\right| = \frac{\pi}{2}\frac{\eta_0}{\lambda}R^3\sqrt{\left\{\begin{array}{l} \dfrac{\left(\lambda\dot{\gamma}_R^0\right)^3}{6}\left[\dfrac{(1-11L)}{(1+L)(1+4L)(1+9L)}\right] \\ -\dfrac{\left(\lambda\dot{\gamma}_R^0\right)^5}{16}\left[\dfrac{(5-130L)}{2(1+L)(1+4L)(1+9L)(1+16L)}\right] \\ +\cdots \end{array}\right\}^2 + \left\{\begin{array}{l} \dfrac{\left(\lambda\dot{\gamma}_R^0\right)^3}{6}\left[\dfrac{6(1-L)\lambda\omega}{(1+L)(1+4L)(1+9L)}\right] \\ -\dfrac{\left(\lambda\dot{\gamma}_R^0\right)^5}{16}\left[\dfrac{(45-120L)\lambda\omega}{2(1+L)(1+4L)(1+9L)(1+16L)}\right] \\ +\cdots \end{array}\right\}^2} \tag{34}$$

$$\left|\mathscr{T}_5\right| = \frac{\pi}{2}\frac{\eta_0}{\lambda}R^3 \sqrt{\left\{-\frac{\left(\lambda\dot{\gamma}_R^0\right)^5}{16}\left[\frac{\left(1-85L+274L^2\right)}{2(1+L)(1+4L)(1+9L)(1+16L)(1+25L)}\right]+\cdots\right\}^2 + \left\{-\frac{\left(\lambda\dot{\gamma}_R^0\right)^5}{16}\left[\frac{\left(15-225L+120L^2\right)\mathrm{De}}{2(1+L)(1+4L)(1+9L)(1+16L)(1+25L)}\right]+\cdots\right\}^2} \tag{35}$$

which we will next use to construct the torque harmonic ratios.

d. Torque Harmonic Ratio

From Eqs. (34) and (33) we can construct the torque ratio:

$$\frac{\left|\mathscr{T}_3\right|}{\left|\mathscr{T}_1\right|} = \frac{\sqrt{\left\{\frac{\left(\lambda\dot{\gamma}_R^0\right)^2}{6}\left[\frac{(1-11L)}{(1+4L)(1+9L)}\right]-\frac{\left(\lambda\dot{\gamma}_R^0\right)^4}{16}\left[\frac{(5-130L)}{2(1+4L)(1+9L)(1+16L)}\right]+\cdots\right\}^2 + \left\{\frac{\left(\lambda\dot{\gamma}_R^0\right)^2}{6}\left[\frac{6(1-L)\lambda\omega}{(1+4L)(1+9L)}\right]-\frac{\left(\lambda\dot{\gamma}_R^0\right)^4}{16}\left[\frac{(45-120L)\lambda\omega}{2(1+4L)(1+9L)(1+16L)}\right]+\cdots\right\}^2}}{\sqrt{\left\{-1+\frac{\left(\lambda\dot{\gamma}_R^0\right)^2}{6}\left[\frac{3}{(1+4L)}\right]-\frac{\left(\lambda\dot{\gamma}_R^0\right)^4}{16}\left[\frac{5}{(1+4L)(1+9L)}\right]+\cdots\right\}^2 + \left\{-\lambda\omega+\frac{\left(\lambda\dot{\gamma}_R^0\right)^2}{6}\left[\frac{6\lambda\omega}{(1+4L)}\right]-\frac{\left(\lambda\dot{\gamma}_R^0\right)^4}{16}\left[\frac{15\lambda\omega}{(1+4L)(1+9L)}\right]+\cdots\right\}^2}} \tag{36}$$

In Eqs. (33)-(35), if we just keep terms up to $\left(\lambda\dot{\gamma}_R^0\right)^3$ we then get:

$$\frac{\left|\mathscr{T}_3\right|}{\left|\mathscr{T}_1\right|} \cong \frac{\sqrt{\left\{\frac{\left(\lambda\dot{\gamma}_R^0\right)^2}{6}(1-11L)\right\}^2 + \left\{\left(\lambda\dot{\gamma}_R^0\right)^2(1-L)\lambda\omega\right\}^2}}{\sqrt{\left\{\left[-(1+4L)+\frac{\left(\lambda\dot{\gamma}_R^0\right)^2}{2}\right](1+9L)\right\}^2 + \left\{\left[-\lambda\omega(1+4L)+\left(\lambda\dot{\gamma}_R^0\right)^2\lambda\omega\right](1+9L)\right\}^2}} \tag{37}$$

Similarly, for the fifth-to-first harmonic ratio of the torque we get:

$$\frac{\left|\mathscr{T}_5\right|}{\left|\mathscr{T}_1\right|}=\frac{\sqrt{\left\{-\frac{\left(\lambda\dot{\gamma}_R^0\right)^4}{16}\left[\frac{\left(1-85L+274L^2\right)}{2(1+4L)(1+9L)(1+16L)(1+25L)}\right]+\cdots\right\}^2+\left\{-\frac{\left(\lambda\dot{\gamma}_R^0\right)^4}{16}\left[\frac{\left(15-225L+120L^2\right)\lambda\omega}{2(1+4L)(1+9L)(1+16L)(1+25L)}\right]+\cdots\right\}^2}}{\sqrt{\left\{-1+\frac{\left(\lambda\dot{\gamma}_R^0\right)^2}{6}\left[\frac{3}{(1+4L)}\right]-\frac{\left(\lambda\dot{\gamma}_R^0\right)^4}{16}\left[\frac{5}{(1+4L)(1+9L)}\right]+\cdots\right\}^2+\left\{-\lambda\omega+\frac{\left(\lambda\dot{\gamma}_R^0\right)^2}{6}\left[\frac{6\lambda\omega}{(1+4L)}\right]-\frac{\left(\lambda\dot{\gamma}_R^0\right)^4}{16}\left[\frac{15\lambda\omega}{(1+4L)(1+9L)}\right]+\cdots\right\}^2}} \tag{38}$$

Eqs. (36) and (38) are plotted in Figure **4** and Figure **5**.

e. Shear Stress Harmonics

From the right side of Eq. (19), we get the amplitudes of each harmonic of the shear stress for cone-plate flow, $\tau_{\theta\phi}$, in large-amplitude oscillatory shear [by analogy with Eqs. (30) through (32)]:

$$\tau_1=\frac{\eta_0}{\lambda}\left[-\left(\lambda\dot{\gamma}^0\right)\frac{\cos\tau+\lambda\omega\sin\tau}{1+L}+\frac{\left(\lambda\dot{\gamma}^0\right)^3}{4}\left[\frac{3\cos\tau+6\lambda\omega\sin\tau}{(1+L)(1+4L)}\right]-\frac{\left(\lambda\dot{\gamma}^0\right)^5}{8}\left[\frac{5\cos\tau+15\lambda\omega\sin\tau}{(1+L)(1+4L)(1+9L)}\right]+\cdots\right] \tag{39}$$

$$\tau_3=\frac{\eta_0}{\lambda}\left[\frac{\left(\lambda\dot{\gamma}^0\right)^3}{4}\left[\frac{(1-11\mathrm{L})\cos3\tau+6(1-L)\lambda\omega\sin3\tau}{(1+L)(1+4L)(1+9L)}\right]-\frac{\left(\lambda\dot{\gamma}^0\right)^5}{8}\left[\frac{(5-130L)\cos3\tau+(45-120L)\lambda\omega\sin3\tau}{2(1+L)(1+4L)(1+9L)(1+16L)}\right]+\cdots\right] \tag{40}$$

$$\tau_5=\frac{\eta_0}{\lambda}\left[-\frac{\left(\lambda\dot{\gamma}^0\right)^5}{8}\left[\frac{\left(1-85L+274L^2\right)\cos5\tau+\left(15-225L+120L^2\right)\lambda\omega\sin5\tau}{2(1+L)(1+4L)(1+9L)(1+16L)(1+25L)}\right]+\cdots\right] \tag{41}$$

We next use Eqs. (39) through (41), to construct expressions for the amplitudes of the shear stress harmonics.

f. Shear Stress Harmonics Amplitude

The amplitudes of the shear stress harmonics are thus [by analogy with Eqs. (33) through (35)] given by:

$$|\tau_1| = \frac{\eta_0}{\lambda}\sqrt{\left[\begin{array}{l} -\left(\lambda\dot{\gamma}^0\right)\dfrac{1}{1+L} \\ \quad +\dfrac{\left(\lambda\dot{\gamma}^0\right)^3}{4}\left[\dfrac{3}{(1+L)(1+4L)}\right] \\ \quad -\dfrac{\left(\lambda\dot{\gamma}^0\right)^5}{8}\left[\dfrac{5}{(1+L)(1+4L)(1+9L)}\right] \\ \quad +\cdots \end{array}\right]^2 + \left[\begin{array}{l} -\left(\lambda\dot{\gamma}^0\right)\dfrac{\lambda\omega}{1+L} \\ \quad +\dfrac{\left(\lambda\dot{\gamma}^0\right)^3}{4}\left[\dfrac{6\lambda\omega}{(1+L)(1+4L)}\right] \\ \quad -\dfrac{\left(\lambda\dot{\gamma}^0\right)^5}{8}\left[\dfrac{15\lambda\omega}{(1+L)(1+4L)(1+9L)}\right] \\ \quad +\cdots \end{array}\right]^2} \tag{42}$$

$$|\tau_3| = \frac{\eta_0}{\lambda}\sqrt{\left[\begin{array}{l} \dfrac{\left(\lambda\dot{\gamma}^0\right)^3}{4}\left[\dfrac{(1-11L)}{(1+L)(1+4L)(1+9L)}\right] \\ \quad -\dfrac{\left(\lambda\dot{\gamma}^0\right)^5}{8}\left[\dfrac{(5-130L)}{2(1+L)(1+4L)(1+9L)(1+16L)}\right] \\ \quad +\cdots \end{array}\right]^2 + \left[\begin{array}{l} \dfrac{\left(\lambda\dot{\gamma}^0\right)^3}{4}\left[\dfrac{6(1-L)\lambda\omega}{(1+L)(1+4L)(1+9L)}\right] \\ \quad -\dfrac{\left(\lambda\dot{\gamma}^0\right)^5}{8}\left[\dfrac{(45-120L)\lambda\omega}{2(1+L)(1+4L)(1+9L)(1+16L)}\right] \\ \quad +\cdots \end{array}\right]^2} \tag{43}$$

$$|\tau_5| = \frac{\eta_0}{\lambda}\sqrt{\left[\begin{array}{l} -\dfrac{\left(\lambda\dot{\gamma}^0\right)^5}{8}\left[\dfrac{\left(1-85L+274L^2\right)}{2(1+L)(1+4L)(1+9L)(1+16L)(1+25L)}\right] \\ \quad +\cdots \end{array}\right]^2 + \left[\begin{array}{l} -\dfrac{\left(\lambda\dot{\gamma}^0\right)^5}{8}\left[\dfrac{\left(15-225L+120L^2\right)\lambda\omega}{2(1+L)(1+4L)(1+9L)(1+16L)(1+25L)}\right] \\ \quad +\cdots \end{array}\right]^2} \tag{44}$$

and we next use Eqs. (42) through (44) to get the shear stress harmonic amplitude ratios.

g. Shear Stress Harmonic Amplitude Ratios

The shear stress harmonic amplitude ratios, for a single relaxation time corotational Maxwell in cone-plate or sliding-plate flow are [by analogy with Eqs. (36) and (38)] then given by:

$$\frac{|\tau_3|}{|\tau_1|}=\frac{\sqrt{\left[\frac{(\lambda\dot\gamma^0)^2}{4}\left[\frac{(1-11L)}{(1+4L)(1+9L)}\right]-\frac{(\lambda\dot\gamma^0)^4}{8}\left[\frac{(5-130L)}{2(1+4L)(1+9L)(1+16L)}\right]+\cdots\right]^2+\left[\frac{(\lambda\dot\gamma^0)^2}{4}\left[\frac{6(1-L)\lambda\omega}{(1+4L)(1+9L)}\right]-\frac{(\lambda\dot\gamma^0)^4}{8}\left[\frac{(45-120L)\lambda\omega}{2(1+4L)(1+9L)(1+16L)}\right]+\cdots\right]^2}}{\sqrt{\left[-1+\frac{(\lambda\dot\gamma^0)^2}{4}\left[\frac{3}{(1+4L)}\right]-\frac{(\lambda\dot\gamma^0)^4}{8}\left[\frac{5}{(1+4L)(1+9L)}\right]+\cdots\right]^2+\left[-\lambda\omega+\frac{(\lambda\dot\gamma^0)^2}{4}\left[\frac{6\lambda\omega}{(1+4L)}\right]-\frac{(\lambda\dot\gamma^0)^4}{8}\left[\frac{15\lambda\omega}{(1+4L)(1+9L)}\right]+\cdots\right]^2}} \tag{45}$$

Eq. is used to plot the amplitude ratio $|\tau_3|/|\tau_1|$ versus $\lambda\dot\gamma^0$ for three values of $\lambda\omega$ in

$$\frac{|\tau_5|}{|\tau_1|}=\frac{\sqrt{\left[-\frac{(\lambda\dot\gamma^0)^4}{8}\left[\frac{(1-85L+274L^2)}{2(1+L)(1+4L)(1+9L)(1+16L)(1+25L)}\right]+\cdots\right]^2+\left[-\frac{(\lambda\dot\gamma^0)^4}{8}\left[\frac{(15-225L+120L^2)\mathrm{De}}{2(1+L)(1+4L)(1+9L)(1+16L)(1+25L)}\right]+\cdots\right]^2}}{\sqrt{\left[-1+\frac{(\lambda\dot\gamma^0)^2}{4}\left[\frac{3}{(1+4L)}\right]-\frac{(\lambda\dot\gamma^0)^4}{8}\left[\frac{5}{(1+4L)(1+9L)}\right]+\cdots\right]^2+\left[-\lambda\omega+\frac{(\lambda\dot\gamma^0)^2}{4}\left[\frac{6\lambda\omega}{(1+4L)}\right]-\frac{(\lambda\dot\gamma^0)^4}{8}\left[\frac{15\lambda\omega}{(1+4L)(1+9L)}\right]+\cdots\right]^2}} \tag{46}$$

Eqs. (45) and (46) are used to plot the amplitude ratios $|\tau_3|/|\tau_1|$ and $|\tau_5|/|\tau_1|$ versus $\lambda\dot\gamma^0$ for three values of $\lambda\omega$ in Figure 6 and Figure 7.

h. Correction to $|\mathscr{T}_3|/|\mathscr{T}_1|$

From (45) and (36), we can construct the third-to-first torque harmonic amplitude correction factor [see Abstract or Table II for the definition of *correction factor*; see also after Eq. (12)]:

$$\frac{|\tau_3|/|\tau_1|}{|\mathscr{T}_3|/|\mathscr{T}_1|}=\sqrt{\frac{\left[\begin{array}{l}\frac{\left(\lambda\dot{\gamma}^0\right)^2}{4}\left[\frac{(1-11L)}{(1+4L)(1+9L)}\right]\\ -\frac{\left(\lambda\dot{\gamma}^0\right)^4}{8}\left[\frac{(5-130L)}{2(1+4L)(1+9L)(1+16L)}\right]\\ +\cdots\end{array}\right]^2+\left[\begin{array}{l}\frac{\left(\lambda\dot{\gamma}^0\right)^2}{4}\left[\frac{6(1-L)\lambda\omega}{(1+4L)(1+9L)}\right]\\ -\frac{\left(\lambda\dot{\gamma}^0\right)^4}{8}\left[\frac{(45-120L)\lambda\omega}{2(1+4L)(1+9L)(1+16L)}\right]\\ +\cdots\end{array}\right]^2}{\left[\begin{array}{l}-1+\frac{\left(\lambda\dot{\gamma}^0\right)^2}{4}\left[\frac{3}{(1+4L)}\right]\\ -\frac{\left(\lambda\dot{\gamma}^0\right)^4}{8}\left[\frac{5}{(1+4L)(1+9L)}\right]\\ +\cdots\end{array}\right]^2+\left[\begin{array}{l}-\lambda\omega+\frac{\left(\lambda\dot{\gamma}^0\right)^2}{4}\left[\frac{6\lambda\omega}{(1+4L)}\right]\\ -\frac{\left(\lambda\dot{\gamma}^0\right)^4}{8}\left[\frac{15\lambda\omega}{(1+4L)(1+9L)}\right]\\ +\cdots\end{array}\right]^2}}{\sqrt{\frac{\left\{\begin{array}{l}\frac{\left(\lambda\dot{\gamma}_R^0\right)^2}{6}\left[\frac{(1-11L)}{(1+4L)(1+9L)}\right]\\ -\frac{\left(\lambda\dot{\gamma}_R^0\right)^4}{16}\left[\frac{(5-130L)}{2(1+4L)(1+9L)(1+16L)}\right]\\ +\cdots\end{array}\right\}^2+\left\{\begin{array}{l}\frac{\left(\lambda\dot{\gamma}_R^0\right)^2}{6}\left[\frac{6(1-L)\lambda\omega}{(1+4L)(1+9L)}\right]\\ -\frac{\left(\lambda\dot{\gamma}_R^0\right)^4}{16}\left[\frac{(45-120L)\lambda\omega}{2(1+4L)(1+9L)(1+16L)}\right]\\ +\cdots\end{array}\right\}^2}{\left\{\begin{array}{l}-1+\frac{\left(\lambda\dot{\gamma}_R^0\right)^2}{6}\left[\frac{3}{(1+4L)}\right]\\ -\frac{\left(\lambda\dot{\gamma}_R^0\right)^4}{16}\left[\frac{5}{(1+4L)(1+9L)}\right]\\ +\cdots\end{array}\right\}^2+\left\{\begin{array}{l}-\lambda\omega+\frac{\left(\lambda\dot{\gamma}_R^0\right)^2}{6}\left[\frac{6\lambda\omega}{(1+4L)}\right]\\ -\frac{\left(\lambda\dot{\gamma}_R^0\right)^4}{16}\left[\frac{15\lambda\omega}{(1+4L)(1+9L)}\right]\\ +\cdots\end{array}\right\}^2}}} \tag{47}$$

In Eqs. (19) and (29), if we just keep terms up to $\left(\lambda\dot{\gamma}^0\right)^5$ and $\left(\lambda\dot{\gamma}_R^0\right)^5$ and then expand in a Taylor series with respect to $\lambda\dot{\gamma}_R^0$ about $\lambda\dot{\gamma}_R^0=0$, we get:

$$\frac{|\tau_3|/|\tau_1|}{|\mathscr{T}_3|/|\mathscr{T}_1|}=\frac{3}{2}+\frac{1}{16}\left[\begin{array}{l}2\left(\frac{\lambda\omega}{(1+L)}\left[\frac{6\lambda\omega}{(1+4L)}\right]+\left[\frac{3}{(1+4L)}\right]\right)\\ -\frac{3\left(\left[6(1-L)\lambda\omega\right]\left[\frac{(45-120L)\lambda\omega}{2(1+16L)}\right]+(1-11L)\left[\frac{(5-130L)}{2(1+16L)}\right]\right)}{\left(\left[6(1-L)\lambda\omega\right]^2+\left[(1-11L)\right]^2\right)}\end{array}\right]\left(\lambda\dot{\gamma}^0\right)^2-\ldots \tag{48}$$

from which we learn that, to zeroth order, the torque amplitude ratio $|\mathscr{T}_3|/|\mathscr{T}_1|$ from rotating parallel-disk flow is attenuated to *about two thirds* of the shear stress amplitude ratio $|\tau_3|/|\tau_1|$ from sliding-plate or cone-plate flow, and (ii) that to the next order, the attenuation will worsen with $\left(\lambda\dot{\gamma}^0\right)^2$, and consequently, the correction factor given by Eq. (48) increases. Since Eq. (19) has been extended to multiple relaxation times (see Eq. (117) in Section 7 of [15]), Eq. (48) can also be so

extended, and thus, where the discrete relaxation spectrum has been determined, torque harmonic amplitudes measured in parallel-disk flow can, with some difficulty, be corrected to their corresponding shear stress harmonic amplitudes (for $\dot{\gamma}^0/\omega$ small enough for the harmonic amplitudes and thus, their ratios, to be fully described with power laws). For steady shear flow (in the limit as $\lambda\omega \to 0$), Eq. (48) gives:

$$\frac{|\tau_3|/|\tau_1|}{|\mathscr{T}_3|/|\mathscr{T}_1|} = \frac{3}{2} + \frac{3}{32}\left(\lambda\dot{\gamma}^0\right)^2 - \ldots = \frac{3}{2}\left(1 + \frac{1}{16}\left(\lambda\dot{\gamma}^0\right)^2 - \ldots\right) \tag{49}$$

In Eqs. (19) and (29), if we just keep terms up to $\left(\lambda\dot{\gamma}^0\right)^3$ and $\left(\lambda\dot{\gamma}_R^0\right)^3$ we get the simpler, cruder approximation to Eq. (48):

$$\frac{|\tau_3|/|\tau_1|}{|\mathscr{T}_3|/|\mathscr{T}_1|} = \frac{3}{2} + \frac{3}{8}\left[\frac{\lambda\omega\left[2\lambda\omega+1\right]}{(L+1)(1+4L)}\right]\left(\lambda\dot{\gamma}^0\right)^2 - \ldots \tag{50}$$

which, for steady shear flow (in the limit as $\lambda\omega \to 0$), gives:

$$\frac{|\tau_3|/|\tau_1|}{|\mathscr{T}_3|/|\mathscr{T}_1|} = \frac{3}{2} \tag{51}$$

the simpler, cruder version of Eq. (49).

Eqs. (48) and (50) are the first *main results* of this work. To a first approximation, Eqs. (48) and (50) agree with Wagner's Eq. (12) above. Eqs. (48) and (50) also demonstrate why the interpretation of torque in oscillatory parallel-disk flow is more complicated than in cone-plate flow.

i. Correction to $|\mathscr{T}_5|/|\mathscr{T}_1|$

Using Eqs. (46) and (38), we can construct the fifth-to-first torque harmonic amplitude correction [see Abstract or Table II for the definition of *correction factor*; see also after Eq. (12)]:

$$\frac{|\tau_5|/|\tau_1|}{|\mathscr{T}_5|/|\mathscr{T}_1|}=\sqrt{\frac{\left[\begin{array}{l}\left[-\frac{\left(\lambda\dot\gamma^0\right)^5}{8}\left[\frac{\left(1-85L+274L^2\right)}{2(1+L)(1+4L)(1+9L)(1+16L)(1+25L)}\right]\right]^2\\ +\left[-\frac{\left(\lambda\dot\gamma^0\right)^5}{8}\left[\frac{\left(15-225L+120L^2\right)\lambda\omega}{2(1+L)(1+4L)(1+9L)(1+16L)(1+25L)}\right]\right]^2\\ +\cdots\end{array}\right]}{\left[\begin{array}{l}\left[-1+\frac{\left(\lambda\dot\gamma^0\right)^2}{4}\left[\frac{3}{(1+4L)}\right]\right]^2+\left[-\lambda\omega+\frac{\left(\lambda\dot\gamma^0\right)^2}{4}\left[\frac{6\lambda\omega}{(1+4L)}\right]\right]^2\\ -\frac{\left(\lambda\dot\gamma^0\right)^4}{8}\left[\frac{5}{(1+4L)(1+9L)}\right]\\ +\cdots\end{array}\right]}}{\left[\begin{array}{l}\left\{-\frac{\left(\lambda\dot\gamma_R^0\right)^5}{16}\left[\frac{\left(1-85L+274L^2\right)}{2(1+L)(1+4L)(1+9L)(1+16L)(1+25L)}\right]\right\}^2\\ +\left\{-\frac{\left(\lambda\dot\gamma_R^0\right)^5}{16}\left[\frac{\left(15-225L+120L^2\right)\lambda\omega}{2(1+L)(1+4L)(1+9L)(1+16L)(1+25L)}\right]\right\}^2\\ +\cdots\end{array}\right]}{\left[\begin{array}{l}\left\{-1+\frac{\left(\lambda\dot\gamma_R^0\right)^2}{6}\left[\frac{3}{(1+4L)}\right]\right\}^2+\left\{-\lambda\omega+\frac{\left(\lambda\dot\gamma_R^0\right)^2}{6}\left[\frac{6\lambda\omega}{(1+4L)}\right]\right\}^2\\ -\frac{\left(\lambda\dot\gamma_R^0\right)^4}{16}\left[\frac{5}{(1+4L)(1+9L)}\right]\\ +\cdots\end{array}\right]}} \tag{52}$$

In Eqs. (19) and (29) and, if we just keep terms up to $\left(\lambda\dot\gamma^0\right)^5$ and $\left(\lambda\dot\gamma_R^0\right)^5$ and then expand in a Taylor series with respect to $\lambda\dot\gamma_R^0$ about $\lambda\dot\gamma_R^0=0$, we get:

$$\frac{|\tau_5|/|\tau_1|}{|\mathscr{T}_5|/|\mathscr{T}_1|}=2+\frac{(2L+1)}{2(L+1)(1+4L)}\left(\lambda\dot\gamma^0\right)^2-\cdots \tag{53}$$

which, in the limit of low frequency $(\lambda\omega\to 0)$, Eq. (53) reduces to:

$$\frac{|\tau_5|/|\tau_1|}{|\mathscr{T}_5|/|\mathscr{T}_1|}=2+\tfrac{1}{4}\left(\lambda\dot\gamma^0\right)^2-\cdots \tag{54}$$

which corresponds to steady shear flow. From Eq. (53), we learn that (i), to zeroth order, the torque amplitude ratio $|\mathscr{T}_5|/|\mathscr{T}_1|$ from parallel-disk flow is attenuated by *about half* of the shear stress amplitude ratio $|\tau_5|/|\tau_1|$ from sliding-plate or cone-plate flow, and (ii) that to the next order, the attenuation will worsen with $\left(\lambda\dot\gamma^0\right)^2$.

Since Eq. (19) has been extended to multiple relaxation times (see Eq. (117) in Section 7 of [15]), Eq. (53) can also be so extended, and thus, where the discrete

relaxation spectrum has been determined, torque harmonic amplitudes measured in parallel-disk flow can be corrected to their corresponding shear stress harmonic amplitudes. Eq. (53) is the second *main result* of this work.

IV. EXPERIMENTAL METHOD

The sample of 1,4-*cis*-polyisoprene used was anionically synthesized in the Karlsruhe laboratory ($M_w = 84{,}000$ g/gmol [59]; PDI $\equiv M_w/M_n = 1.04$ [59]; $M_e = 4{,}000$ g/gmol [60]; $T_g = -61.7°C$ measured using differential scanning calorimetry [61]). It is an entangled [$M_w/M_e = 21$ entanglements per chain], nearly monodisperse, linear homopolymer melt. The real part, $\eta'(\omega)$, and minus the imaginary part, $\eta''(\omega)$, of the complex viscosity, $\eta^*(\omega)$, were measured in parallel-disk flow using small-amplitude oscillatory shear flow with $R = 8.0\,\text{mm}$ and $h = 0.5\,\text{mm}$ [62,63] at $T = 52.8°C$ with $\dot{\gamma}^0/\omega < 0.01$, and we present these results in Figure **18**.

Our large-amplitude oscillatory shear flow measurements were performed on an ARES-G2 strain controlled rheometer (*TA Instruments*, 159 Lukens Drive, New Castle, DE 19720) using parallel disks ($R = 5.0$ mm, plate-partitioning gap in stationary plate of 0.1 mm, outer plate radius 5.1 mm) and cone-plate ($R = 5.0$ mm, $\left(\frac{\pi}{2} - \theta_c\right) = 0.099$ rad) geometries. For both the parallel-disk and cone-plate flow experiments, we used a stationary disk following the single-partition design of Fig. 1 of [64]). We chose plate-partitioning to allow measurements up to higher shear rate amplitudes (without the offending effects of edge distortion and fracture) [65,66,67,68]. We find plate-partitioning to be an excellent alternative to sliding plate rheometry incorporating a local shear stress transducer in the stationary plate [69,70,71,72,73,74].In the large-amplitude oscillatory shear flow experiments, the sample was subjected to a series of oscillations with increasing strain amplitude $\left(\dot{\gamma}^0/\omega\right)_o$ at a fixed angular frequency of $\omega = 6.3$ rad/s and at $T = 52.8°C$. The temperature was controlled with a forced convection air bath. The strain amplitude range was $0.01 < \dot{\gamma}^0/\omega < 3$ and was chosen to span both the linear as well as the nonlinear region. For each amplitude, 25 cycles were recorded by oversampling [75] in the time domain using the commercial TRIOS software provided by *TA Instruments*. The first 2 cycles of the sampled time data for each strain amplitude were discarded, to ensure *alternance* [15], so that cycles 3 through 27 were then analyzed for each point in Figure **10** through Figure **17**. Also, each data set in Figure **10** through Figure **17** represents a pair of separate sample loadings. For the Fourier transform of the time data, a custom MATLAB [*MathWorks*, 3 Apple Hill Drive, Natick, MA 01760-2098] code was used to get the amplitudes of the shear stress harmonics, $|\tau_1|$, $|\tau_3|$ and $|\tau_5|$, and also of the torque harmonics, $|\mathscr{T}_1|$, $|\mathscr{T}_3|$ and $|\mathscr{T}_5|$, from the corresponding measured time series [76].

V. THEORY VERSUS MEASUREMENT

For the third-to-first $|\tau_3|/|\tau_1|$ measurements (where $\lambda\dot{\gamma}^0 > 0.05$) we find Eq. (45) to fit at $\lambda = 0.0158\text{s}$ (see Figure **10**). The value $\lambda = 0.0158\text{s}$ compares with the value of $\lambda \equiv 1/\omega_c = 0.011\text{s}$ deduced from the crossover frequency, ω_c [where $G'(\omega_c) = G''(\omega_c)$] reported in **Table 1** and in **Figs. 2 a)** and **b)** of [59]. Hence, the PI-84k, in cone-plate flow, seems to obey the single relaxation time corotational Maxwell model, include the slope of 2 [and thus the scaling exponent implied by Eq. (45)]. Using the same value of $\lambda = 0.0158\text{s}$, for the $|\mathscr{T}_3|/|\mathscr{T}_1|$ measurements (where $\lambda\dot{\gamma}_R^0 > 0.05$), we then get agreement with Eq. (36) (see Figure **12**). In other words, the PI-84k, in parallel-disk flow, seems to obey the corotational Maxwell model too. In Figure **14**, for the $|\mathscr{T}_3|/|\mathscr{T}_1|$ and $|\tau_3|/|\tau_1|$ measurements (where $\lambda\dot{\gamma}_R^0 > 0.05$ and $\lambda\dot{\gamma}^0 > 0.05$), we confirm the first main result of this paper, that is, that the correction factor for parallel-disk flow is indeed $\left(|\tau_3|/|\tau_1|\right)/\left(|\mathscr{T}_3|/|\mathscr{T}_1|\right) = \frac{3}{2}$ [from Eq. (50)].

In Figure **15**, for the $|\mathscr{T}_5|/|\mathscr{T}_1|$ and $|\tau_5|/|\tau_1|$ measurements (where $\lambda\dot{\gamma}_R^0 > 0.2$ and $\lambda\dot{\gamma}^0 > 0.2$), we confirm the second main result of this paper, that is, that the correction factor for parallel-disk flow is indeed $\left(|\tau_5|/|\tau_1|\right)/\left(|\mathscr{T}_5|/|\mathscr{T}_1|\right) = 2$ [from Eq.(53)]. .

For the fifth-to-first $|\mathscr{T}_5|/|\mathscr{T}_1|$ measurements (where $\lambda\dot{\gamma}_R^0 > 0.2$) we find a match for the slope [and thus the scaling exponent implied by Eq. (46)] of four predicted by Eq. (38) at $\lambda = 0.0158\text{s}$ (see Figure **13**). In other words, the PI-84k, in parallel-disk flow, seems to match the slope predicted by the corotational Maxwell model, but the model falls well below the measured values of $|\mathscr{T}_5|/|\mathscr{T}_1|$. Using $\lambda = 0.0158\text{s}$, for the $|\tau_5|/|\tau_1|$ measurements (where $\lambda\dot{\gamma}^0 > 0.2$), we again find a match for the slope of four predicted by Eq. (45) (see Figure **11**). In other words, the PI-84k, in cone-plate flow, seems to match the slope of the corotational Maxwell model, but the model falls below the measured values of $|\tau_5|/|\tau_1|$. In Figure **15**, for the $|\mathscr{T}_5|/|\mathscr{T}_1|$ and $|\tau_5|/|\tau_1|$ measurements (where $\lambda\dot{\gamma}_R^0 > 0.2$ and $\lambda\dot{\gamma}^0 > 0.2$), we confirm the second main result of this paper, that is, that the correction factor for parallel-disk flow is indeed $\left(|\tau_5|/|\tau_1|\right)/\left(|\mathscr{T}_5|/|\mathscr{T}_1|\right) = 2$.

VI. CONCLUSION

We find that parallel-disk flow attenuates the third-to-first harmonic ratio by a factor of $\frac{2}{3}$, and the fifth-to-first, by a factor of $\frac{1}{2}$. By *attenuates* we mean that the torque harmonic amplitude ratios fall below the corresponding shear stress amplitude ratios that would be measured in cone-plate or sliding-plate flow, and specifically, that $\left|\mathscr{T}_3\right|/\left|\mathscr{T}_1\right| < \left|\tau_3\right|/\left|\tau_1\right|$ and $\left|\mathscr{T}_5\right|/\left|\mathscr{T}_1\right| < \left|\tau_5\right|/\left|\tau_1\right|$. In this work, we have compared the higher harmonics of the torque, measured in oscillatory parallel-disk flow, with the higher harmonics of the shear stress, and measured in cone-plate flow. We use an analytical solution for the corotational Maxwell model to arrive at two simple correction factors, one for the amplitude ratio of the third-to-first torque harmonics, and another for the fifth-to-first. We find that data measured in the parallel-disk flow and corrected using, the factor of $\frac{3}{2}$ for the third-to-first [Eq. (50)], and 2 for the fifth-to-first [Eq. (53)], agree with our oscillatory cone-plate flow measurements for 1,4-*cis*-polyisoprene.

Further, our expression for the torque in large-amplitude oscillatory parallel-disk flow [Eq. (22), with Eqs. (23) through (28), is also useful for the design of the simplest of torsional viscous dampers, consisting of a viscoelastic liquid between two disks.

VII. APPENDIX: SHEAR RATE CORRECTION

An alternative approach to correcting torque measurements from parallel-disk flow is to try to adjust the shear rate at the rim to match a corresponding value for the cone-plate measurement. For the power-law fluid in parallel-disk flow:

$$\tau_{\theta z} = -m\left[\frac{\partial v_\theta}{\partial z} + \frac{1}{r}\frac{\partial v_z}{\partial \theta}\right]^n = -m\left(\frac{\partial v_\theta}{\partial z}\right)^n \tag{55}$$

and substituting Eq. (3) into Eq. (55) gives:

$$\tau_{\theta z} = -m\left(\frac{\partial}{\partial z}\left[\Omega r\left(z/h\right)\right]\right)^n = -m\left[\frac{\Omega r}{h}\right]^n \tag{56}$$

and substituting Eq. (56) into Eq. (6) gives:

$$\begin{aligned}\mathscr{T} &= 2\pi m\left[\frac{\Omega}{h}\right]^n \int_0^R r^{2+n}\,dr \\ &= 2\pi m\left[\frac{\Omega R}{h}\right]^n \frac{R^3}{3+n} \\ &= \frac{2\pi m R^3}{3+n}\dot{\gamma}_R^n\end{aligned} \tag{57}$$

For cone-plate flow, the torque that the fluid exerts on the plate is given by:

$$\begin{aligned}\mathscr{T} &= -\int_0^{2\pi}\int_0^R r\cdot\tau_{\theta\phi} r\left(\sin\tfrac{\pi}{2}\right)dr\,d\phi \\ &= -2\pi\int_0^R \tau_{\theta\phi} r^2\,dr\end{aligned} \tag{58}$$

and the shear stress for cone-plate flow, for a power-law fluid, is given by:

$$\tau_{\theta\phi} = -m\left[\frac{\Omega}{\left(\frac{\pi}{2}-\theta_c\right)}\right]^n = -m\dot{\gamma}_c^n \tag{59}$$

Substituting Eq. (59) into Eq. (58):

$$\begin{aligned}\mathscr{T} &= 2\pi m\dot{\gamma}_c^n\int_0^R r^2\,dr \\ &= \frac{2\pi m}{3}R^3\dot{\gamma}_c^n\end{aligned} \tag{60}$$

Equating Eqs. (57) and (60), and then rearranging gives the final expression for the power-law correction factor:

$$\frac{\dot{\gamma}_c}{\dot{\gamma}_R} = \left[\frac{3}{3+n}\right]^{1/n} \tag{61}$$

From Eq. (61) we learn that, for shear-thinning power-law fluids, the correction factor is bounded by:

$$\tfrac{1}{\sqrt[3]{e}} \le \left(\dot{\gamma}_c/\dot{\gamma}_R\right) \le \tfrac{3}{4} \tag{62}$$

or approximately, by $0.7165 \le \left(\dot{\gamma}_c/\dot{\gamma}_R\right) \le 0.75$ In other words, for shear-thinning power-law fluids, the correction factor $\dot{\gamma}_c/\dot{\gamma}_R$ *hardly departs from its Newtonian value* (by only -4%). From Eq. (61) we learn that $\dot{\gamma}_c/\dot{\gamma}_R$ does not approach the Newtonian value $\frac{3}{4}$ asymptotically, but rather with the low slope of:

$$\left.\frac{d\left(\dot{\gamma}_c/\dot{\gamma}_R\right)}{dn}\right|_{n=1} = \tfrac{3}{4}\left(\log\tfrac{4}{3}-\tfrac{3}{4}\right) \cong 0.03 \tag{63}$$

In Figure **19** we illustrate the interesting behavior of the correction factor given by Eq. (61).

For the special case of a Newtonian fluid, where $n=1$, Eq. (61) gives:

$$\dot{\gamma}_c = \tfrac{3}{4}\dot{\gamma}_R \tag{64}$$

which has already been tested experimentally and verified for $\left|\mathscr{T}_3\right|/\left|\mathscr{T}_1\right|$ for $\dot{\gamma}^0/\omega \le 1$ for a solution of polyisobutylene in oligoisobutylene. (see Figs. 4a and 4b of [26]), but this correction then did not work for $\dot{\gamma}^0/\omega > 1$. In other words, for some systems, one can accomplish the same correction as our new Eq. (51), however, Figure 16 shows that for the $\left|\mathscr{T}_3\right|/\left|\mathscr{T}_1\right|$ data collected in this work, Eq.

(64) is unsatisfactory. Curiously, Figure 17 shows that Eq. (64) did work well for the $\left|\mathscr{T}_5\right|/\left|\mathscr{T}_1\right|$ data collected for our 1,4-*cis*-polyisoprene.

For our 1,4-*cis*-polyisoprene, from the inflection point to the $\left|\eta^*(\omega)\right|$ curve (and applying the Cox-Merz rule [77]) we measure:

$$n \equiv \left.\frac{d\log\left|\eta^*(\omega)\right|}{d\log\omega}\right|_{\omega_i} = \left.\frac{d\log\eta(\dot{\gamma})}{d\log\dot{\gamma}}\right|_{\dot{\gamma}_i=\omega_i} = 0.685 \tag{65}$$

where ω_i is the angular frequency at the inflection of the $\log\left|\eta^*(\omega)\right|$ versus $\log\dot{\gamma}$ curve at $T = 52.8°C$. Substituting Eq. (65) into Eq. (61), gives the power-law correction for our 1,4-*cis*-polyisoprene of $\dot{\gamma}_c/\dot{\gamma}_R = 0.741$ which hardly differs from the Newtonian correction of $\frac{3}{4}$ that we illustrate in Figure **16** and Figure **17**, which are discussed above. For alternative treatments of correction factors for the shear rate in parallel-disk flow see Section 5.5 of [78] and also [79,80,81]).

VIII. ACKNOWLEDGMENT

AJG acknowledges the Ontario/Baden-Württemberg Exchange Program for the Faculty Research Exchange 2014-2015 award. AJG is also indebted to Professor Manfred Wilhelm of the Institut fuer Technische und Polymerchemie of the Karlsruhe Institute of Technology in Germany for hosting his Visiting Professorship during the summer of 2014. A.J. Giacomin is indebted to the Faculty of Applied Science and Engineering of Queen's University at Kingston, for their support through a Research Initiation Grant (RIG).

IX. DEDICATION

To Professor and Doctor Gerald G. Fuller of the Department of Chemical Engineering of Stanford University, on the occasion of his receiving the degree of *doctor honoris causa*, conferred by the Catholic University of Leuven in Belgium (June 3, 2014).

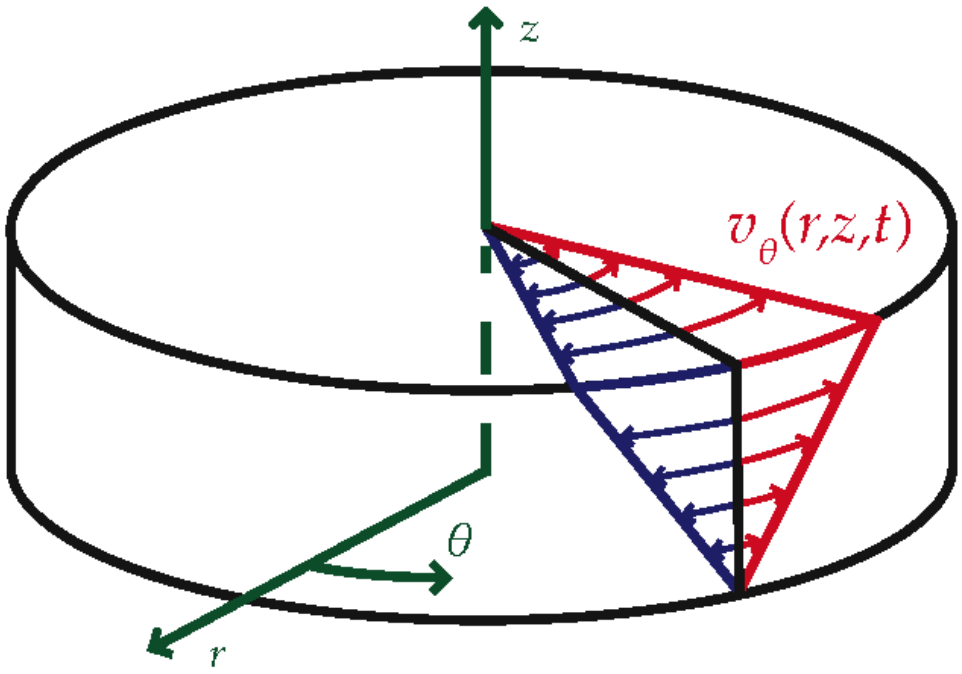

Figure 1: Orthomorphic sketch of parallel-disk flow rheometer fixture. Cylindrical coordinates (r,θ,z) with origin on the stationary disk. The linear velocity profile, $v_\theta = \Omega r(z/h)$, results from the assumption that inertial effects can be neglected.

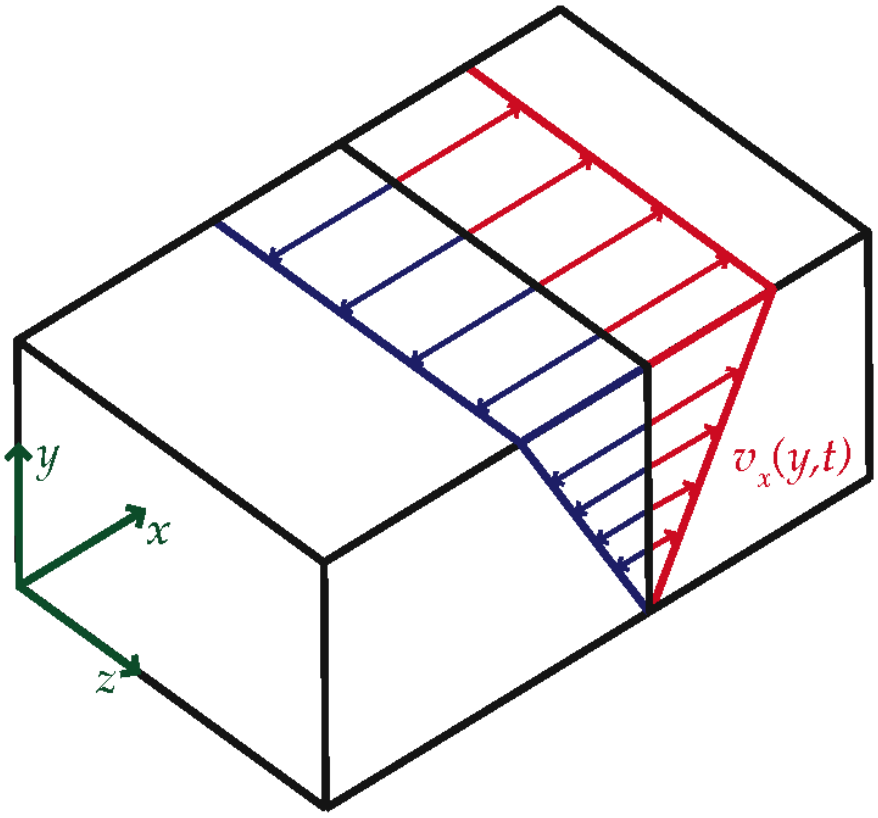

Figure 2: Orthomorphic isometric sketch of alternating velocity profile in oscillatory shear flow between stationary and moving plates of the sliding-plate geometry [Eq. (6)]. Cartesian coordinates with origin on the stationary plate. The linear velocity profile, $v_x = Vy/h$, results from the assumption that inertial effects can be neglected.

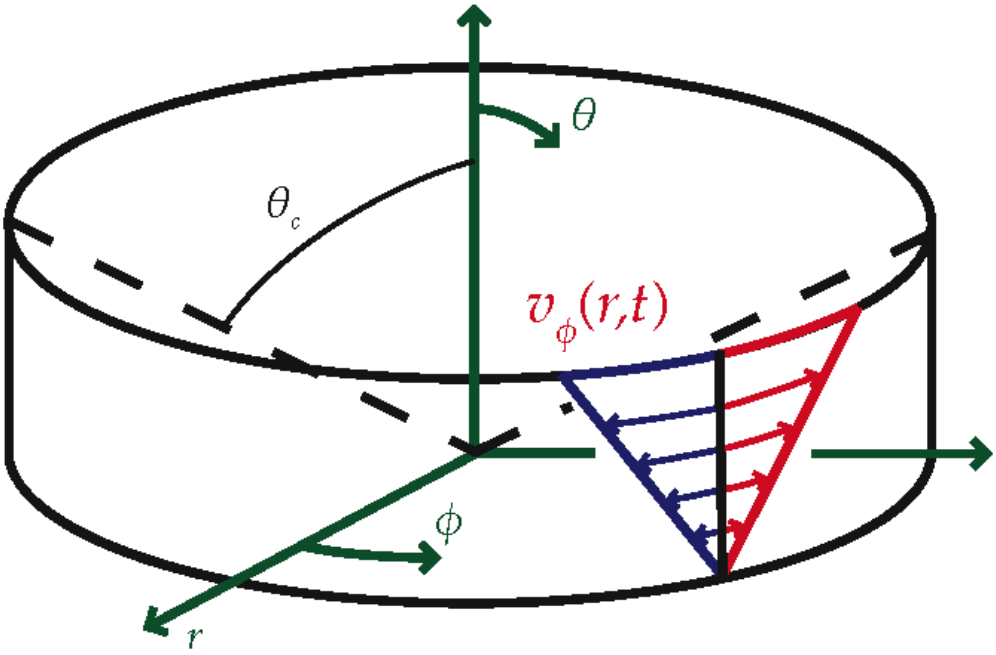

Figure 3: Orthomorphic sketch of cone-plate flow rheometer fixture. Spherical coordinates (r,θ,ϕ) with origin at the cone apex. The linear velocity profile, $v_\phi = \Omega r\left[\left(\frac{\pi}{2}-\theta\right)/\left(\frac{\pi}{2}-\theta_c\right)\right]$, results from the assumption that inertial effects can be neglected, and applies to shallow cones, where $\sin\left(\frac{\pi}{2}-\theta_c\right) \ll 1$.

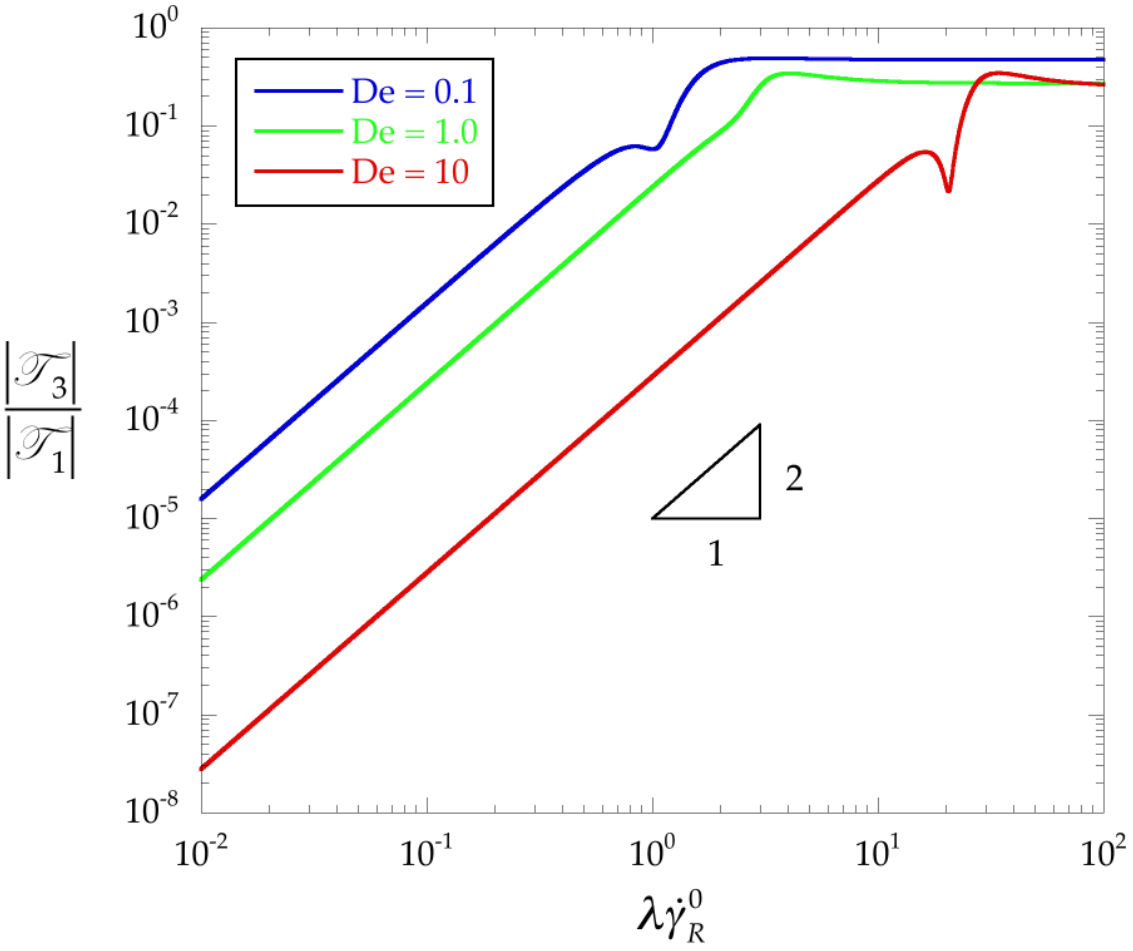

Figure 4: Third-to-first torque harmonic amplitude ratio $|\mathscr{T}_3|/|\mathscr{T}_1|$ versus $\lambda\dot{\gamma}^0$ for $\lambda\omega = \frac{1}{10}, 1, 10$ [Eq. (36)].

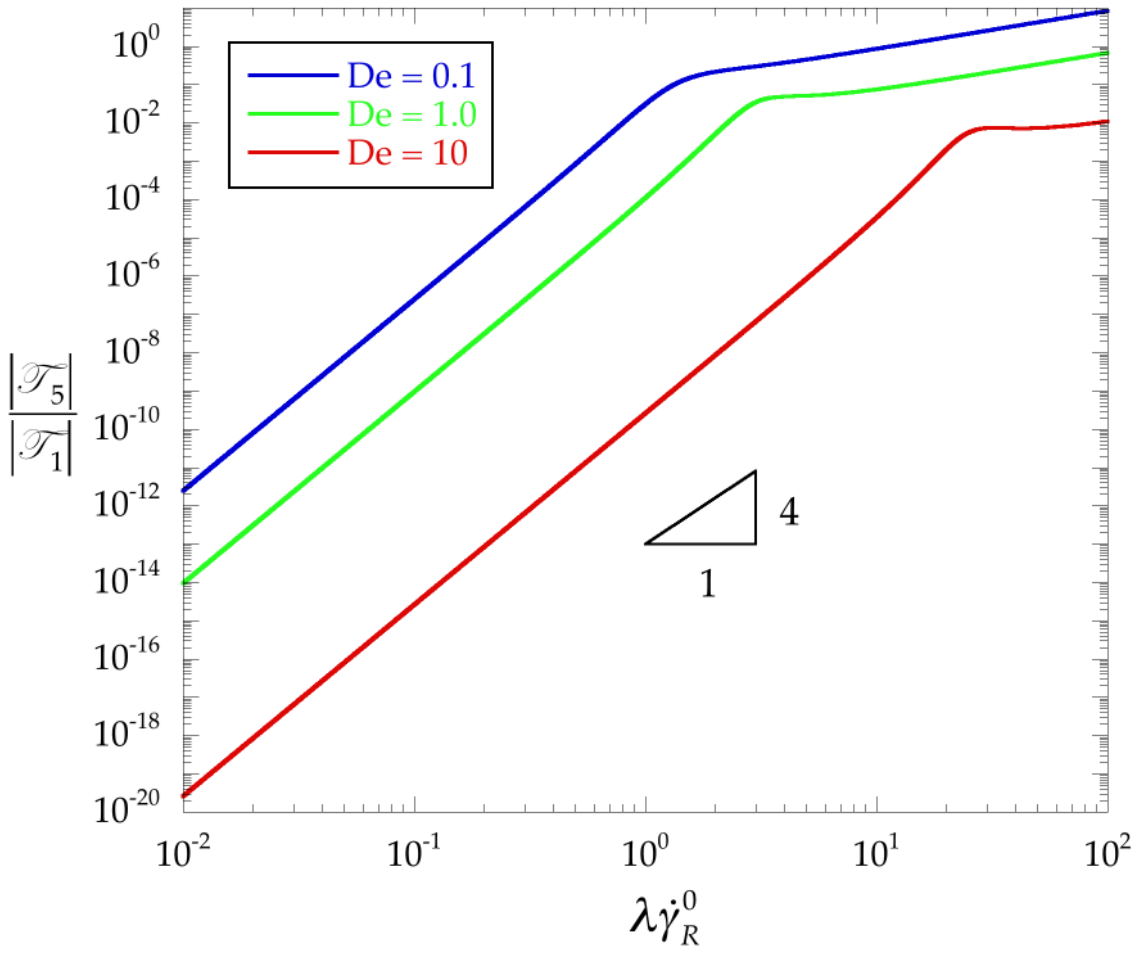

Figure 5: Fifth-to-first torque harmonic amplitude ratio $|\mathscr{T}_5|/|\mathscr{T}_1|$ versus $\lambda\dot{\gamma}^0$ for $\lambda\omega = \frac{1}{10}, 1, 10$ [Eq. (38)].

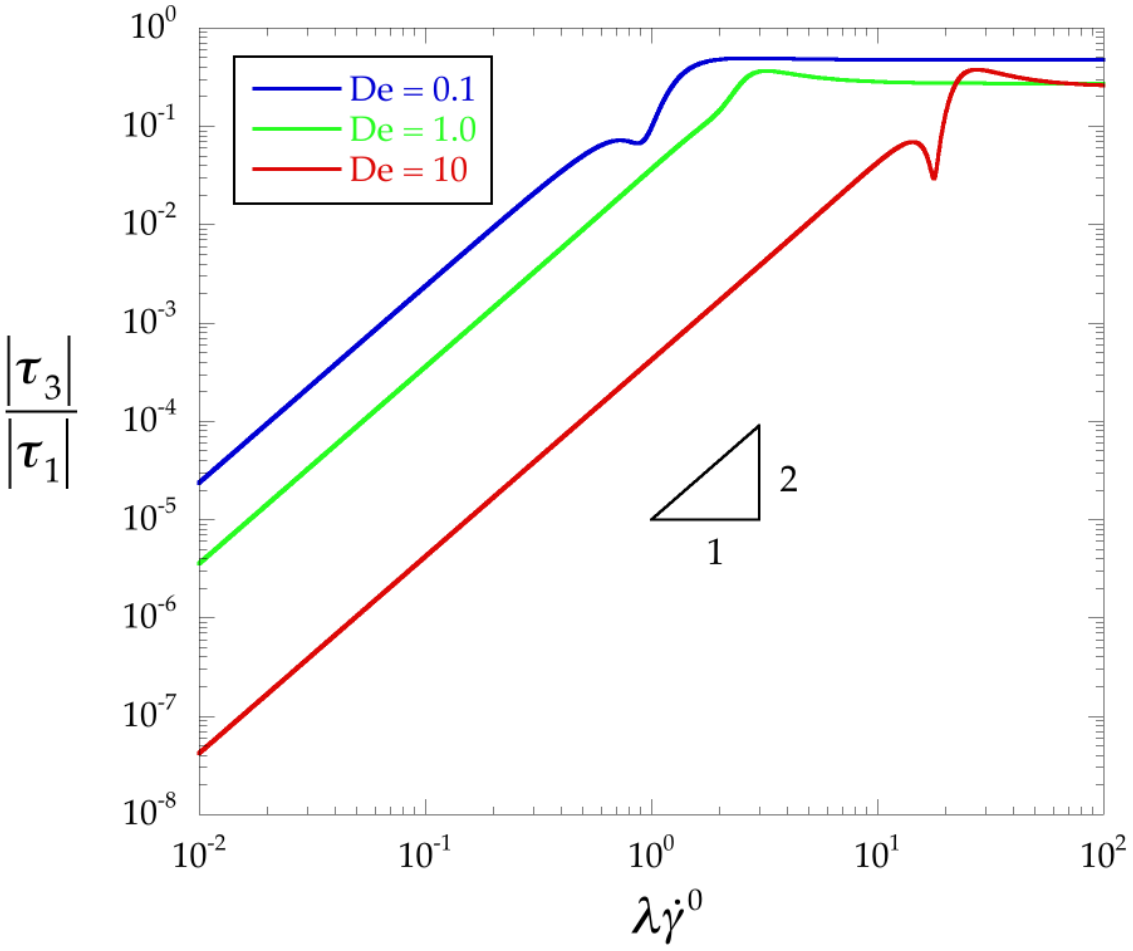

Figure 6: Third-to-first shear stress harmonic amplitude ratio $|\tau_3|/|\tau_1|$ versus $\lambda\dot{\gamma}^0$ for $\lambda\omega = \frac{1}{10}, 1, 10$ [Eq. (45)].

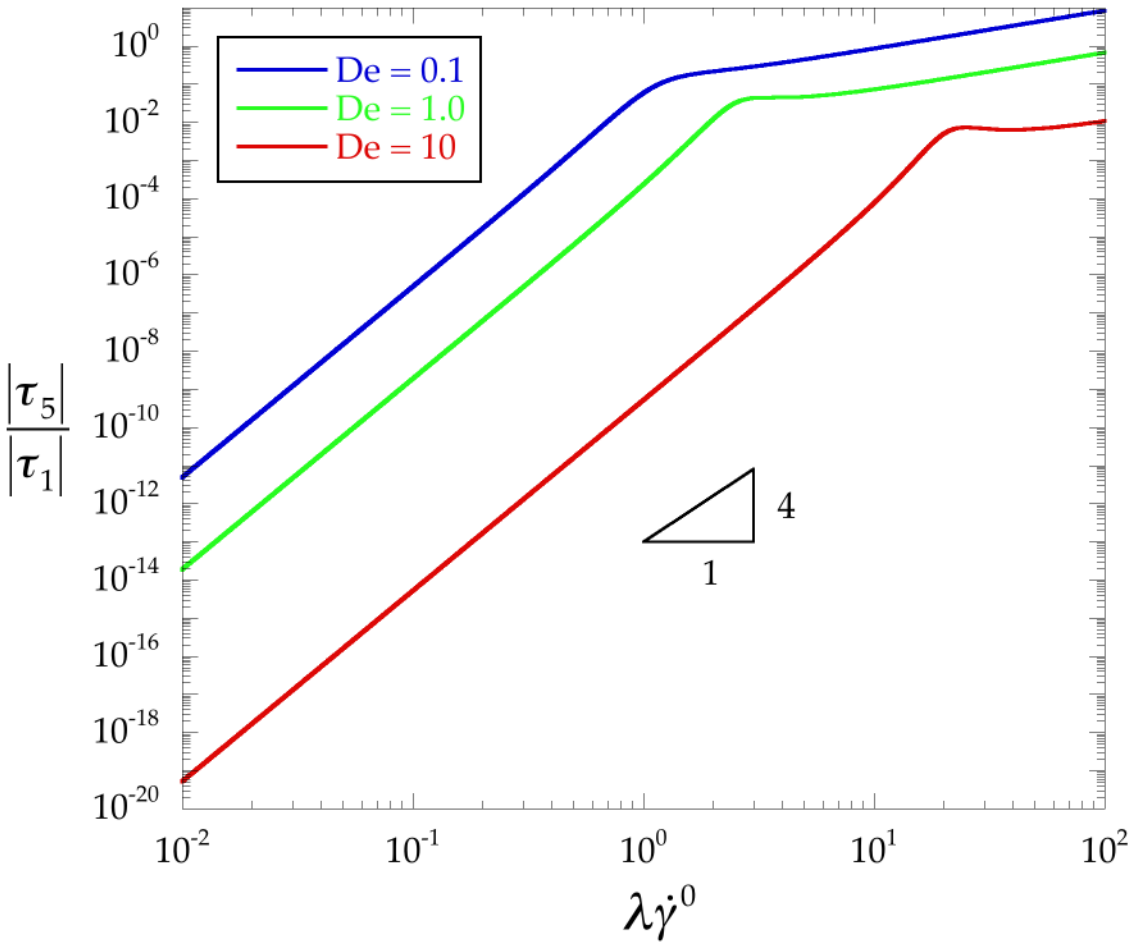

Figure 7: Fifth-to-first shear stress harmonic amplitude ratio $|\tau_5|/|\tau_1|$ versus $\lambda\dot{\gamma}^0$ for $\lambda\omega = \frac{1}{10}, 1, 10$ [Eq. (46)].

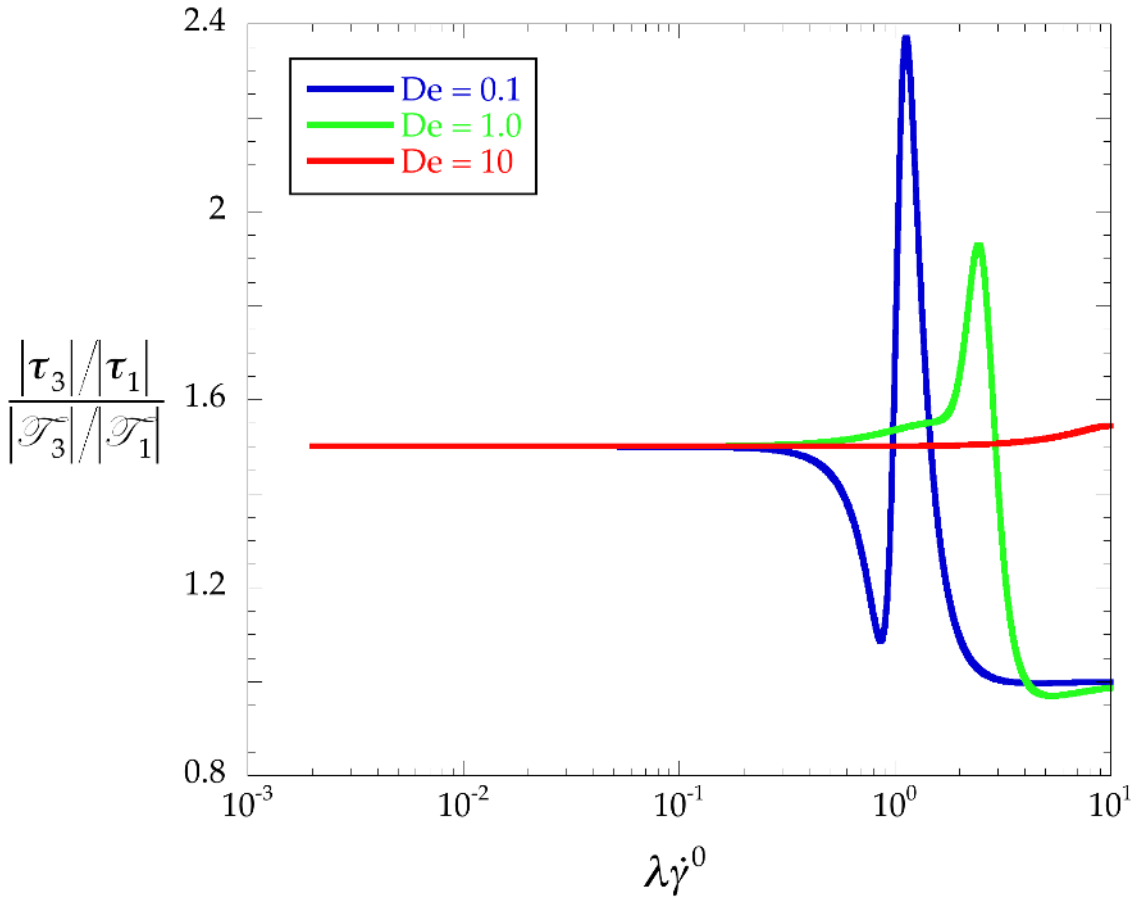

Figure 8: Third-to-first harmonic amplitude ratio correction for torque measured in parallel-disk flow $\left(|\tau_3|/|\tau_1|\right)/\left(|\mathscr{T}_3|/|\mathscr{T}_1|\right)$ versus $\lambda\dot{\gamma}^0$ for $\lambda\omega = \frac{1}{10}, 1, 10$ [Eq. (47)]; the correction approaches $3/2$ at low $\lambda\dot{\gamma}^0$.

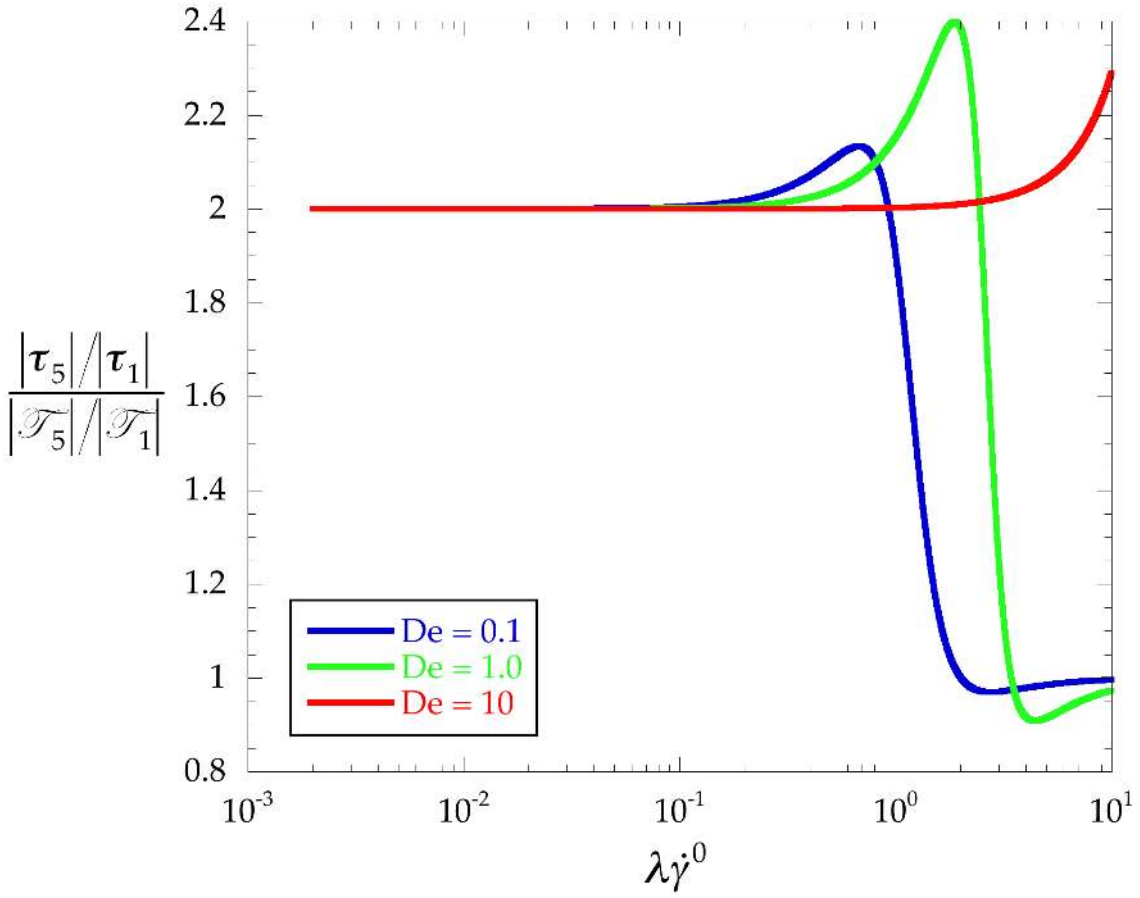

Figure 9: Fifth-to-first harmonic amplitude ratio correction for torque measured in parallel-disk flow $\left(|\tau_5|/|\tau_1|\right)/\left(|\mathscr{T}_5|/|\mathscr{T}_1|\right)$ versus $\lambda\dot{\gamma}^0$ for $\lambda\omega = \frac{1}{10}, 1, 10$ [Eq. (52)]; the correction approaches 2 at low $\lambda\dot{\gamma}^0$.

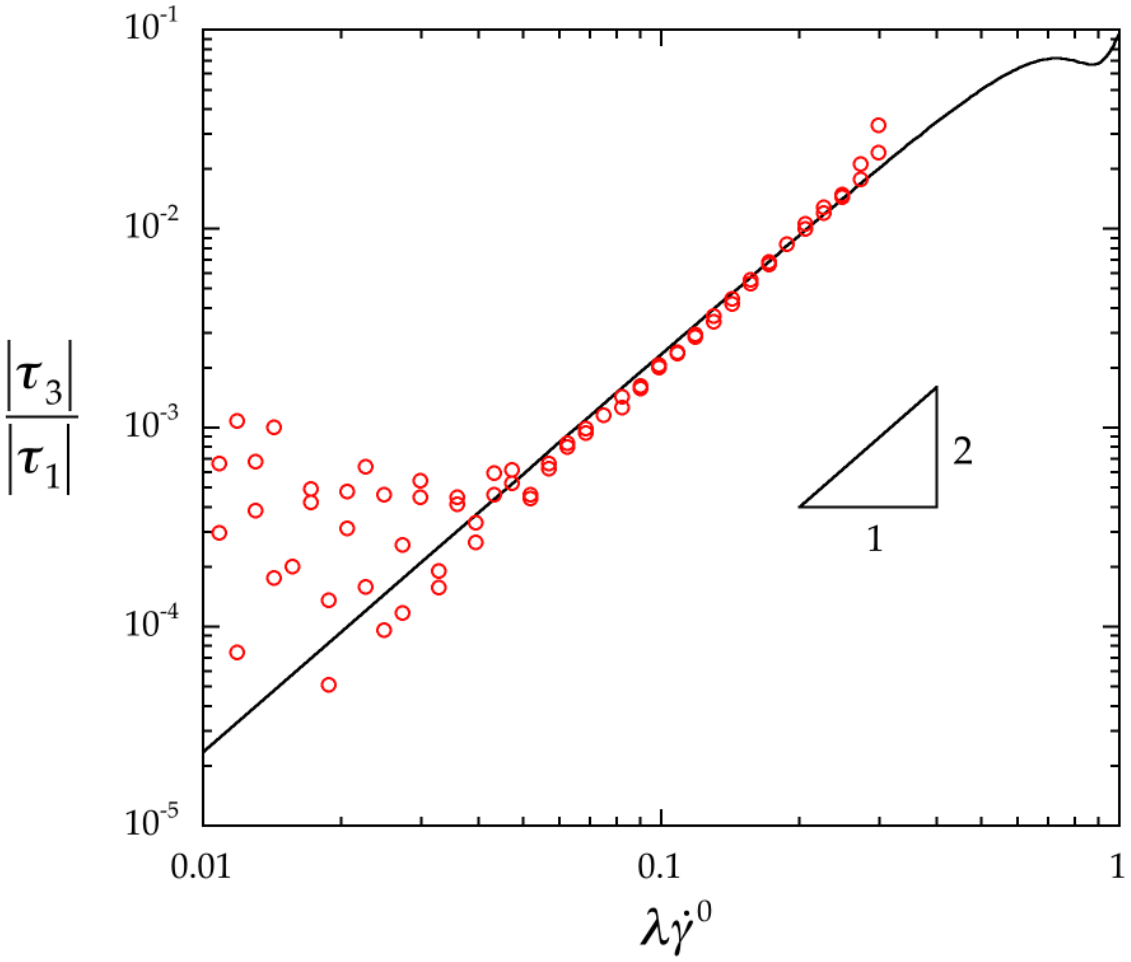

Figure 10: Third-to-first shear stress harmonic amplitude ratio $|\tau_3|/|\tau_1|$ versus $\lambda\dot{\gamma}^0$ for $\lambda\omega = 0.0998$ ($\lambda = 0.0158$s obtained by fitting corotational Maxwell model (solid curve), Eq. (45), to these data. For 1,4-*cis*-polyisoprene, $\omega = 2\pi$ rad/s, T = 52.8°C, cone-plate flow measurements.

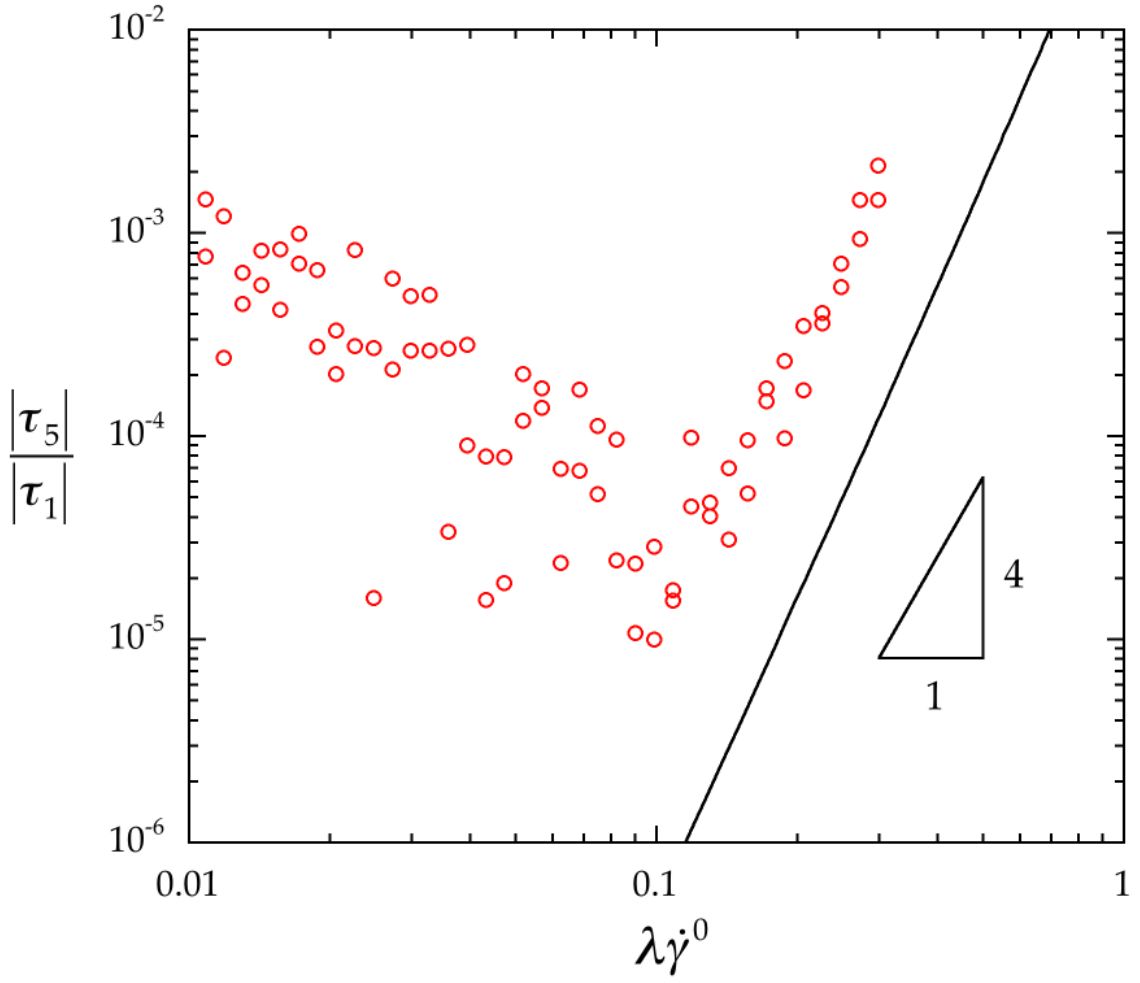

Figure 11: Fifth-to-first shear stress harmonic amplitude ratio $|\tau_5|/|\tau_1|$ versus $\lambda\dot{\gamma}^0$ for $\lambda\omega = 0.0998$ (using fitted value of $\lambda = 0.0158\,\text{s}$; $\omega = 2\pi\,\text{rad/s}$) [solid curve is for corotational Maxwell model, from Eq. (45)]. For 1,4-*cis*-polyisoprene, $T = 52.8°\text{C}$, cone-plate flow measurements.

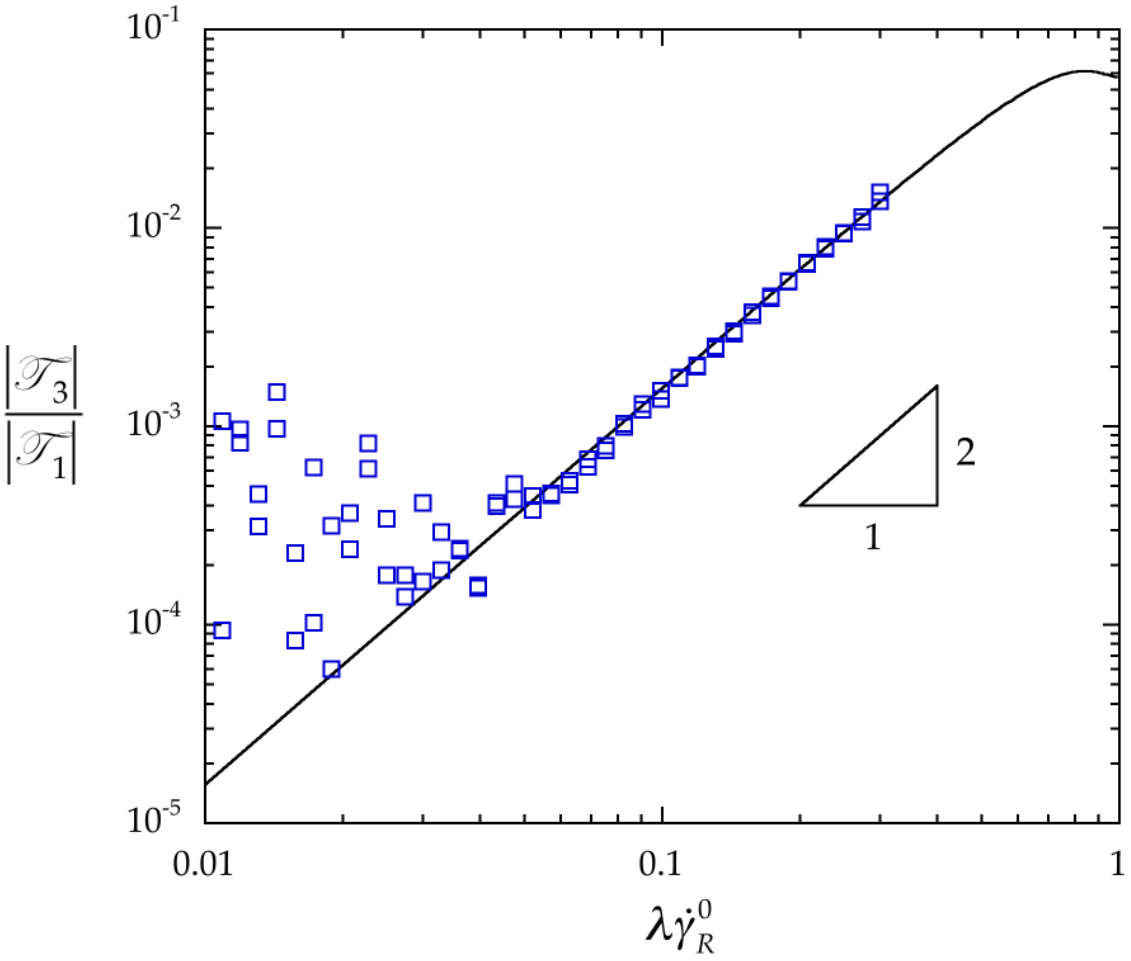

Figure 12: Third-to-first torque harmonic amplitude ratio $\left|\mathscr{T}_3\right| / \left|\mathscr{T}_1\right|$ versus $\lambda\dot{\gamma}^0$ for $\lambda\omega = 0.0998$ (using fitted value of $\lambda = 0.0158\,\text{s}$; $\omega = 2\pi\,\text{rad/s}$) [solid curve is for parallel disk flow of corotational Maxwell fluid, from Eq. (36)]. For 1,4-*cis*-polyisoprene, T = 52.8°C, parallel-disk flow measurements.

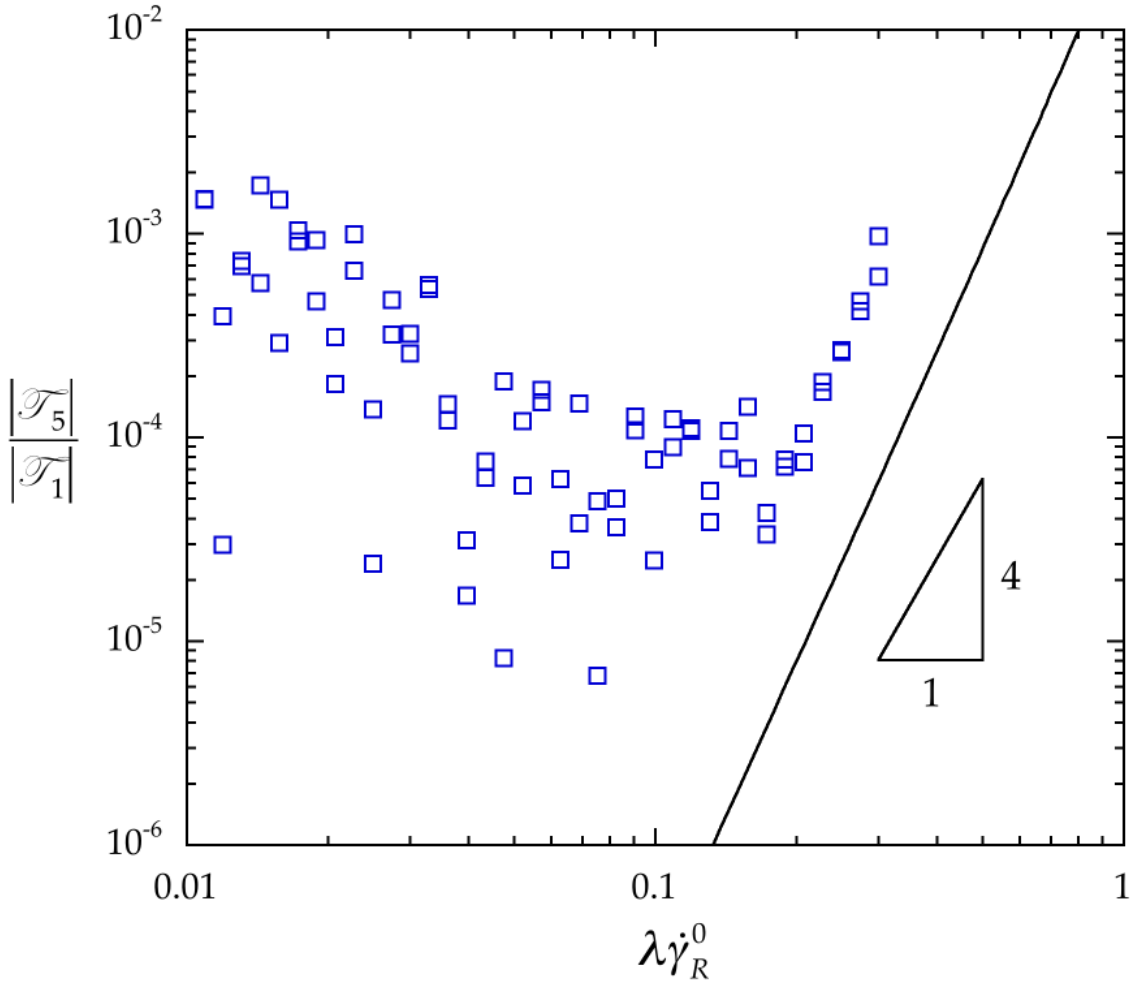

Figure 13: Fifth-to-first torque harmonic amplitude ratio $|\mathscr{T}_5|/|\mathscr{T}_1|$ versus $\lambda\dot{\gamma}^0$ for $\lambda\omega = 0.0998$ (using fitted value of $\lambda = 0.0158\,\text{s}$; $\omega = 2\pi\,\text{rad/s}$) [solid curve is for parallel disk flow of corotational Maxwell fluid, from Eq. (38)]. For 1,4-*cis*-polyisoprene, T = 52.8°C, parallel-disk flow measurements.

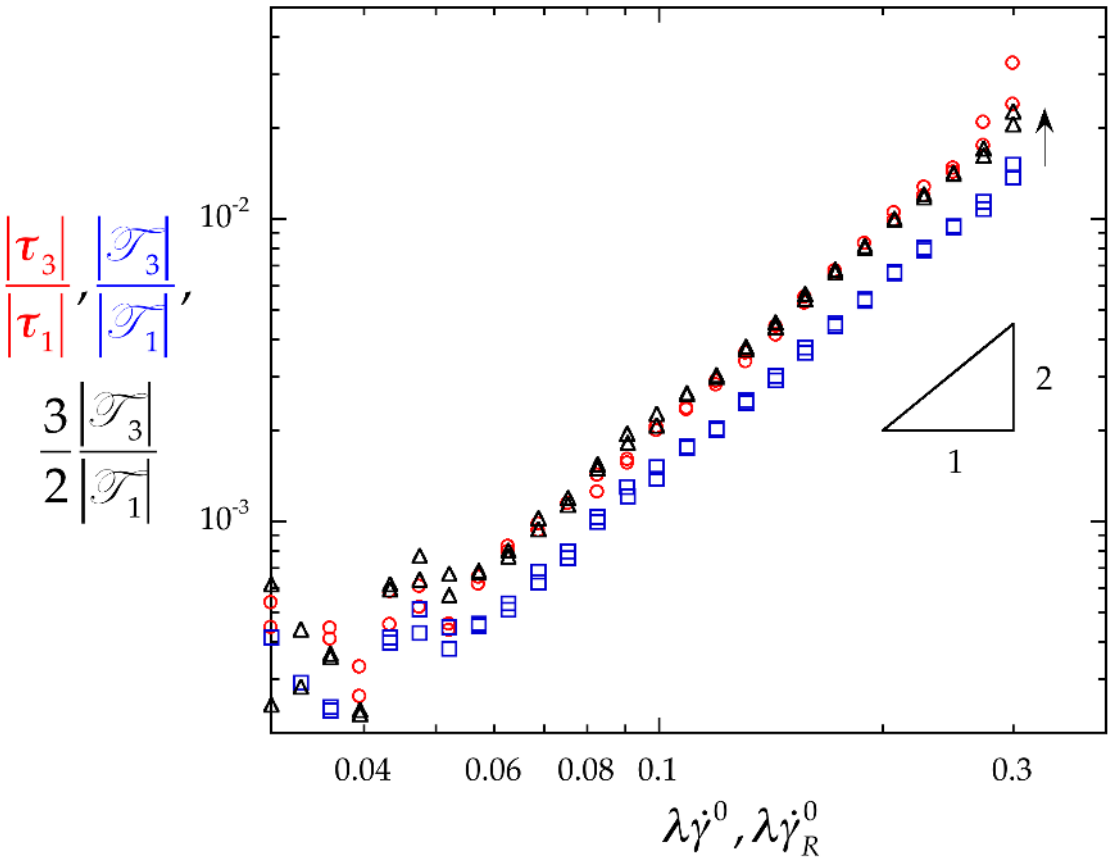

Figure 14: Measured third-to-first shear stress amplitude ratio, $|\tau_3|/|\tau_1|$, (open circles) versus $\lambda\dot{\gamma}^0$, and torque harmonic amplitude ratio $|\mathcal{T}_3|/|\mathcal{T}_1|$ versus $\lambda\dot{\gamma}^0_R$ (open squares), and also using the correction from Eq. (48), $\frac{3}{2}|\mathcal{T}_3|/|\mathcal{T}_1|$ versus $\lambda\dot{\gamma}^0_R$ (open triangles). Arrow shows direction of correction from open squares to **open triangles**. For 1,4-*cis*-polyisoprene, T = 52.8°C .

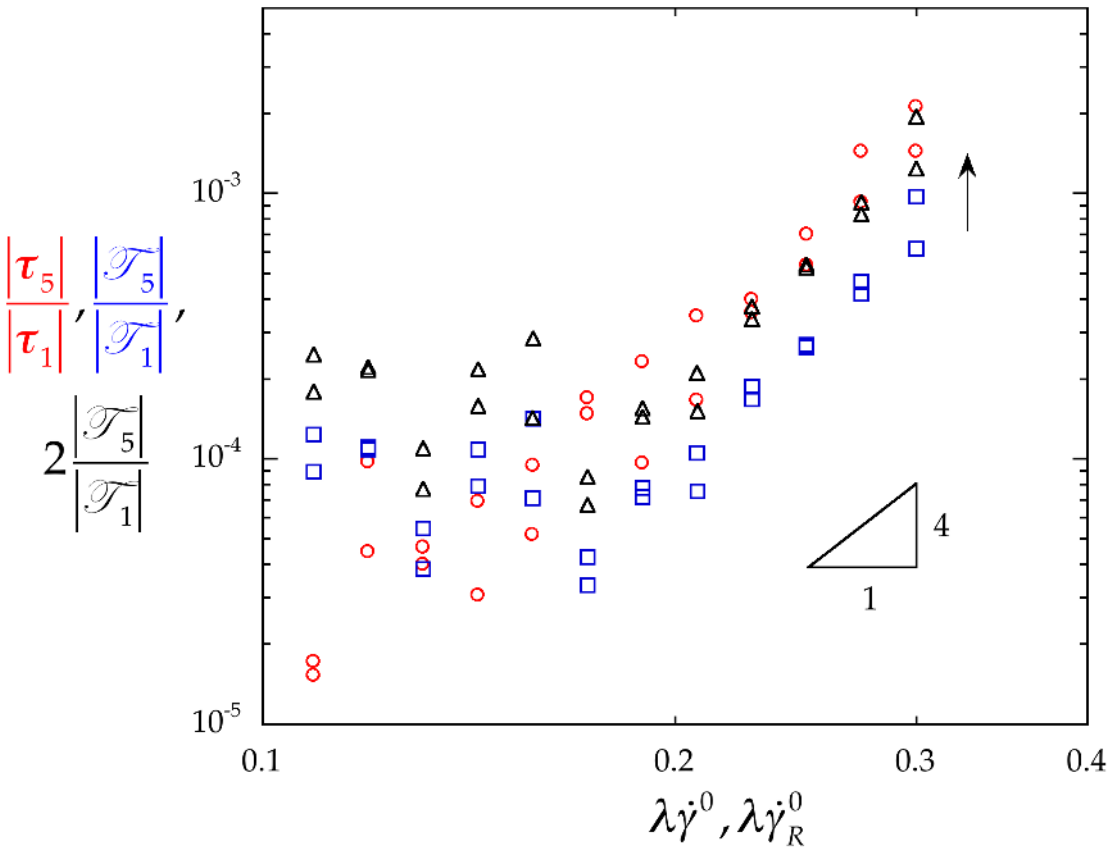

Figure 15: Measured fifth-to-first shear stress amplitude ratio, $|\tau_5|/|\tau_1|$, (open circles) versus $\lambda\dot{\gamma}^0$, and torque harmonic amplitude ratio $|\mathscr{T}_5|/|\mathscr{T}_1|$ versus $\lambda\dot{\gamma}^0_R$ (open squares), and also using the correction from Eq. (48), $2|\mathscr{T}_5|/|\mathscr{T}_1|$ versus $\lambda\dot{\gamma}^0_R$ (**open triangles**). Arrow shows direction of correction from open squares to **open triangles**. For 1,4-*cis*-polyisoprene, T = 52.8°C .

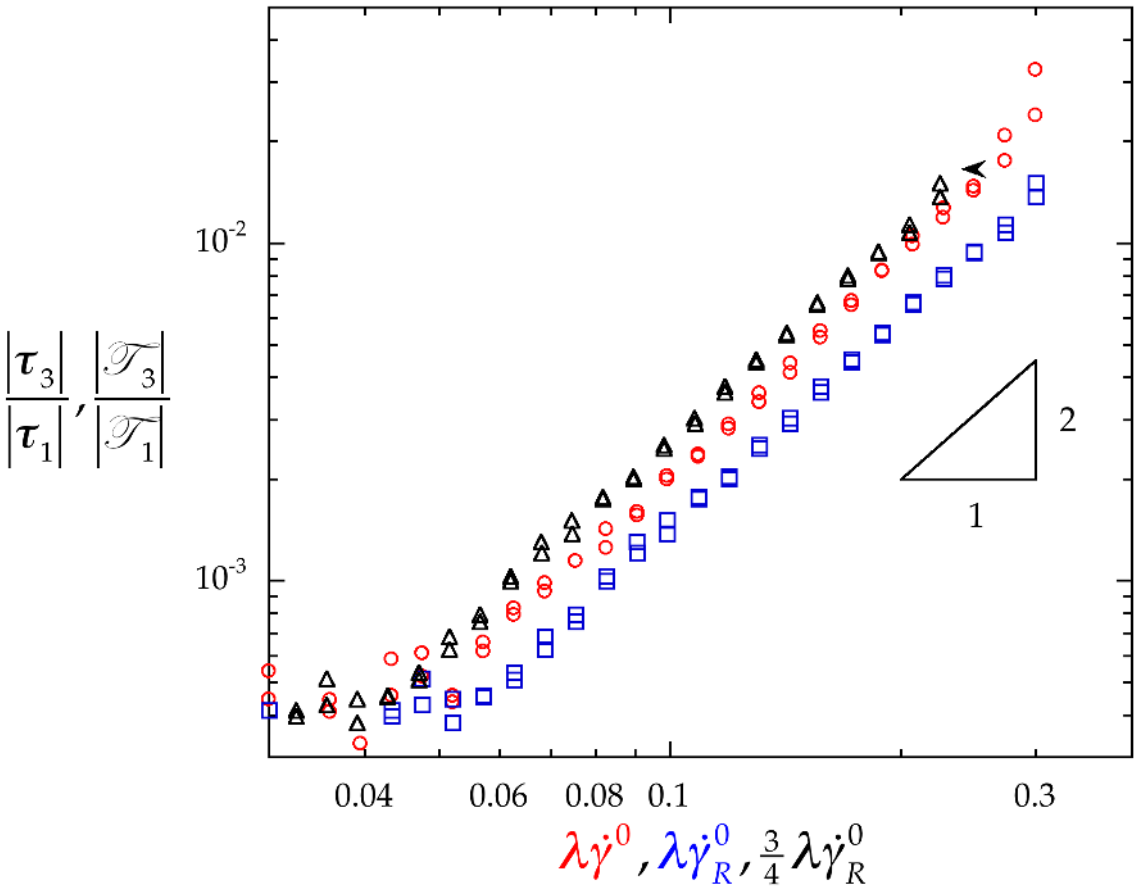

Figure 16: Measured third-to-first shear stress amplitude ratio, $|\tau_3|/|\tau_1|$, (open circles) versus $\lambda\dot{\gamma}^0$, and torque harmonic amplitude ratio $|\mathscr{T}_3|/|\mathscr{T}_1|$ versus $\lambda\dot{\gamma}^0_R$ (open squares), and also versus the Newtonian, and power-law corrections, $\frac{3}{4}\lambda\dot{\gamma}^0_R$ (open triangle) and $\left[3/(3+n)\right]^{1/n}\lambda\dot{\gamma}^0_R$ (open diamonds). For 1,4-*cis*-polyisoprene, T = 52.8°C .

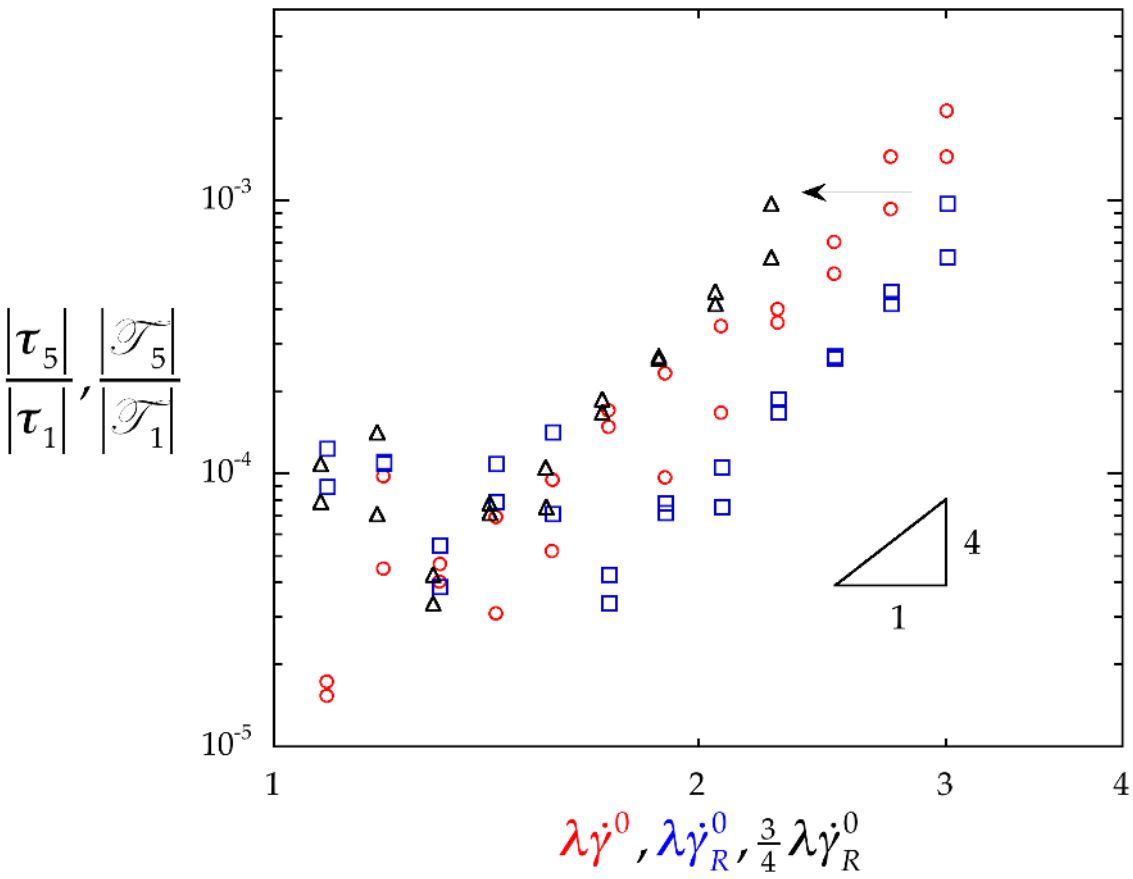

Figure 17: Measured fifth-to-first shear stress amplitude ratio, $|\tau_5|/|\tau_1|$, (open circles) versus $\lambda\dot{\gamma}^0$, and torque harmonic amplitude ratio $|\mathscr{T}_5|/|\mathscr{T}_1|$ versus $\lambda\dot{\gamma}^0_R$ (open squares), and also versus the Newtonian correction, $\frac{3}{4}\lambda\dot{\gamma}^0_R$ (open triangle). For 1,4-*cis*-polyisoprene, T = 52.8°C .

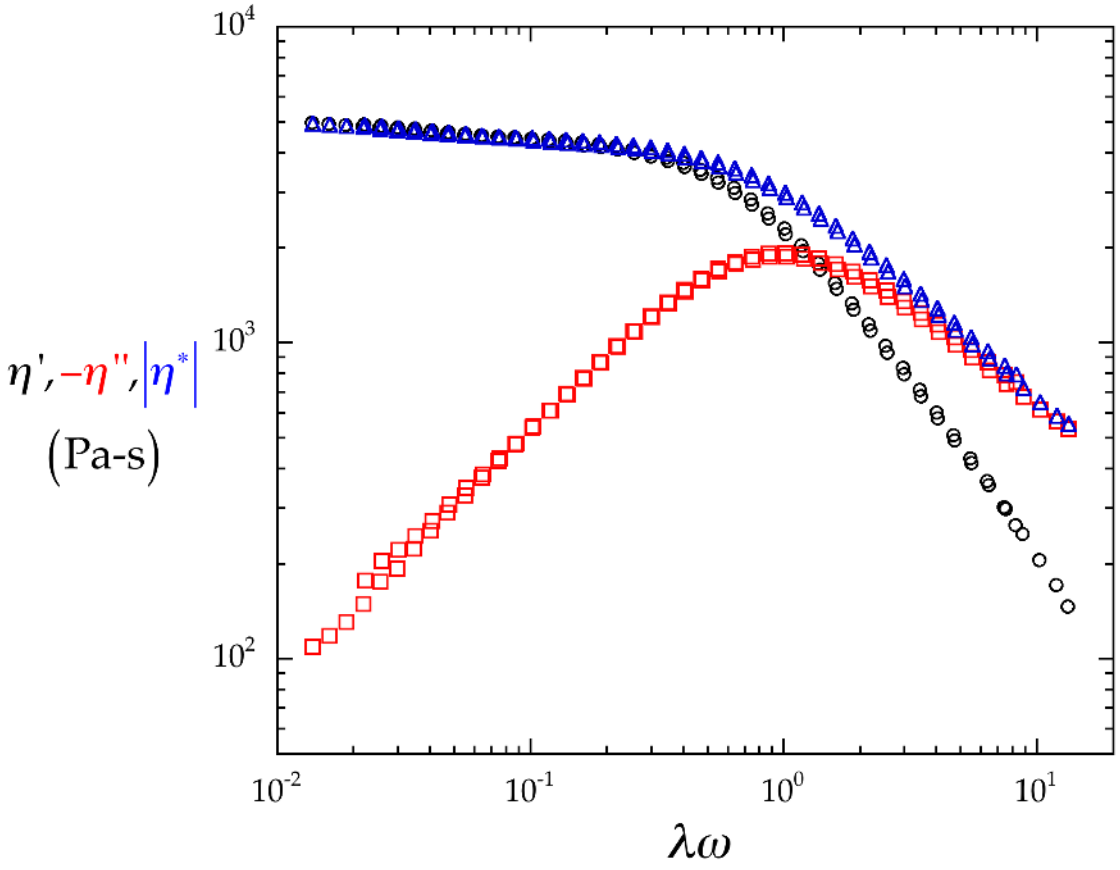

Figure 18: Real part, $\eta'(\omega)$ [**black circles**] and minus the imaginary part, $\eta''(\omega)$ [red squares], of the complex viscosity, $\eta^*(\omega)$ [blue triangles] measured in parallel-disk flow using small-amplitude oscillatory shear *versus* frequency, ω, made dimensionless with $\lambda = 0.0158\,\mathrm{s}$ (from fitting Eq. (45) to data in Figure 10). For 1,4-*cis*-polyisoprene, T = 52.8°C.

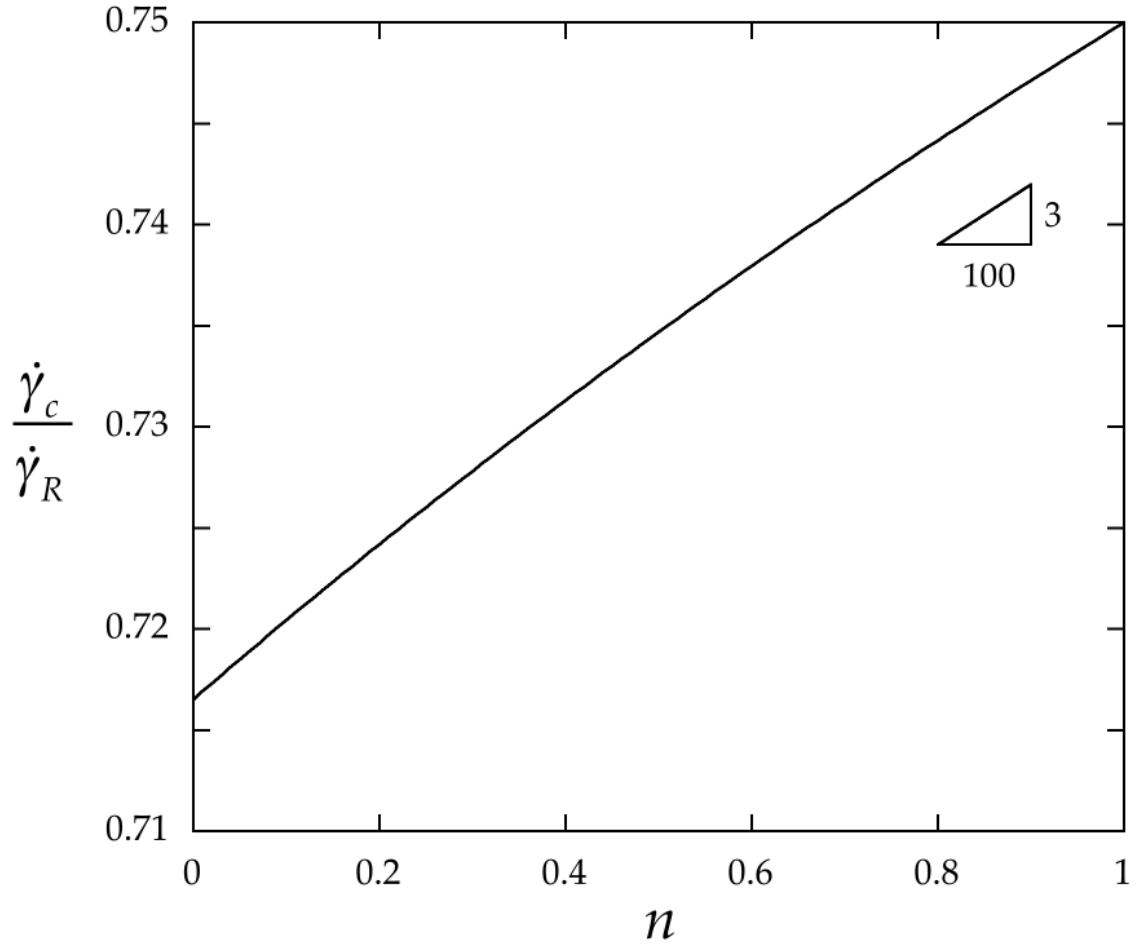

Figure 19: Correction factor $\dot{\gamma}_c/\dot{\gamma}_R$ *versus* power-law index n using Eq. (61): $\dot{\gamma}_c/\dot{\gamma}_R = \left[3/(3+n)\right]^{1/n}$. For shear-thinning fluids, the correction factor is bounded by $\frac{1}{\sqrt[3]{e}} \le \left(\dot{\gamma}_c/\dot{\gamma}_R\right) \le \frac{3}{4}$.

Table I: Dimensional Variables

Name	Symbol	Dimensions	Range
Angular rate of displacement amplitude	Ω^0	t^{-1}	≥ 0
Angular test frequency	ω	t^{-1}	≥ 0
Angular test frequency at the inflection of the $\lvert\eta^*(\omega)\rvert$ curve	ω_i	t^{-1}	≥ 0
Cartesian coordinate, distance from stationary plate (Figure **2**)	y	L	$\mathbb{R}$
Cartesian coordinate, flow direction (Figure **2**)	x	L	$\mathbb{R}$
Cartesian coordinate, transverse to flow direction (Figure **2**)	z	L	$\mathbb{R}$
Characteristic time for fluid	λ	t	≥ 0
Cone angle	θ_0	rad	$0 \leq \theta < 2\pi$
Corotational derivative	$\frac{\mathscr{D}}{\mathscr{D}t}$	t^{-1}	$\mathbb{R}$
Cylindrical coordinate, angular, flow direction (Figure **1**)	θ	rad	$0 \leq \theta < 2\pi$
Cylindrical coordinate, distance from stationary plate (Figure **1**)	z	L	$\mathbb{R}$
Cylindrical coordinate, radial, transverse to flow direction (Figure **1**)	r	L	≥ 0
Extra stress tensor*, ij – component	$\boldsymbol{\tau}_{ij}$	M/Lt^2	$\mathbb{R}$

Loss viscosity of mnth order	η''_{mn}	Mt^{n-2}/L	≥ 0
Molecular weight, weight average	M_w	$M/mole$	≥ 0
Molecular weight, number average	M_n	$M/mole$	≥ 0
Molecular weight, entanglement	M_e	$M/mole$	≥ 0
Nonlinear loss modulus, mnth order	G''_{mn}	Mt^{m-2}/L	$\mathbb{R}$
Nonlinear storage modulus, mnth order	G'_{mn}	Mt^{m-2}/L	$\mathbb{R}$
Parallel-disk gap	h	L	≥ 0
Parallel-disk radius	R	L	≥ 0
Power-law coefficient	m	Mt^{n-2}/L	≥ 0
Rate of deformation tensor	$\dot{\boldsymbol{\gamma}}$	t^{-1}	$\mathbb{R}$
Rate of deformation tensor*, ij – component	$\dot{\gamma}_{ij}$	t^{-1}	$\mathbb{R}$
Shear rate amplitude	$\dot{\gamma}^0$	t^{-1}	≥ 0
Shear rate amplitude at parallel-disk rim	$\dot{\gamma}^0_R$	t^{-1}	$\mathbb{R}$
Shear rate at inflection of steady shear viscosity curve, $\eta(\dot{\gamma})$	$\dot{\gamma}_i$	t^{-1}	≥ 0
Shear rate, steady shear flow	$\dot{\gamma}$	t^{-1}	≥ 0
Shear stress harmonic amplitude, hth	$\lvert\boldsymbol{\tau}_h\rvert$	M/Lt^2	≥ 0
Shear stress harmonic, hth	$\boldsymbol{\tau}_h$	M/Lt^2	$\mathbb{R}$
Spherical coordinate, angle from axis (Figure **3**)	θ	rad	$0 \leq \theta \leq \pi$
Spherical coordinate, flow direction (Figure **3**)	ϕ	rad	$0 \leq \phi < 2\pi$
Spherical coordinate, transverse to flow direction (Figure **3**)	r	L	≥ 0

Steady shear viscosity function	$\eta(\dot{\gamma})$	M/Lt	≥ 0
Storage viscosity of mn th order	η'_{mn}	Mt^{n-2}/L	≥ 0
Temperature	T	T	≥ 0
Temperature, glass transition	T_g	T	≥ 0
Time	t	t	≥ 0
Torque	$\mathscr{T}$	ML^2/t^2	$\mathbb{R}$
Torque harmonic amplitude, hth	$\lvert\mathscr{T}_h\rvert$	ML^2/t^2	≥ 0
Torque harmonic, hth	$\mathscr{T}_h$	ML^2/t^2	$\mathbb{R}$
Torque harmonic, nth order contribution term of the hth	$\mathscr{T}_{h,n}$	ML^2/t^2	$\mathbb{R}$
Velocity gradient tensor	$\nabla\mathbf{v}$	t^{-1}	$\mathbb{R}$
Velocity vector	$\mathbf{v}$	L/t	$\mathbb{R}$
Velocity, ith component	v_i	L/t	$\mathbb{R}$
Vorticity tensor	$\boldsymbol{\omega}$	t^{-1}	$\mathbb{R}$
Zero shear viscosity	η_0	M/Lt	≥ 0

Legend: $M \equiv$ mass; $L \equiv$ length; $t \equiv$ time; $T \equiv$ temperature

* Where τ_{ij} is the force exerted in the jth direction on a unit area of fluid surface of constant x_i by fluid in the region lesser x_i on fluid in the region greater x_i [43].

**See Eqs. (4.4-14) and (4.4-15) and also NOTATION FOR VOLUME 1: Greek Symbols of [44].

Table II: Dimensionless Variables and Groups

Name	Symbol	Range
Correction factor for measured torque amplitude ratios, hth -to-first	$\left(\lvert\tau_h\rvert/\lvert\tau_1\rvert\right)/\left(\lvert\mathscr{T}_h\rvert/\lvert\mathscr{T}_1\rvert\right)$	≥ 0
Deborah number squared	$L \equiv (\lambda\omega)^2$	≥ 0
Deborah number, oscillatory shear	$\lambda\omega$	≥ 0
Harmonic number	h	≥ 0
Intrinsic Nonlinearity	$Q_0^{h/1}$	≥ 0
Natural logarithm	log	≥ 0
Power-law index	n	≥ 0
Shear stress harmonic amplitude ratio, hth -to-first	$I_{h/1} \equiv \lvert\tau_h\rvert/\lvert\tau_1\rvert$	≥ 0
Time	ωt	$\mathbb{R}$
Torque harmonic amplitude ratio, hth -to-first	$\lvert\mathscr{T}_h\rvert/\lvert\mathscr{T}_1\rvert$	≥ 0
Weissenberg number, oscillatory parallel-disk flow	$\lambda\dot{\gamma}_R^0$	≥ 0
Weissenberg number, oscillatory shear flow	$\lambda\dot{\gamma}^0$	≥ 0

Legend: $\mathbb{R} \equiv$ all real numbers

X. REFERENCES

[1] Bird, R.B. and A.J. Giacomin, "Who conceived the complex viscosity?," *Rheologica Acta*, **51**(6), 481-486 (2012).

[2] Hyun, K., M. Wilhelm, C.O. Klein, K.S. Cho, J.G. Nam, K.H. Ahn, S.J. Lee, R.H. Ewoldt, G.H. McKinley, "A review of nonlinear oscillatory shear tests: Analysis and application of large amplitude oscillatory shear (LAOS)," *Progress in Polymer Science*, **36**, 1697–1753 (2011).

[3] Yosick, J.A. and A.J. Giacomin, "Can nonlinear deformation amplify subtle differences in linear viscoelasticity?," *Journal of Non-Newtonian Fluid Mechanics*, **66**, 193-212 (1996).

[4] Giacomin, A.J., R.S. Jeyaseelan and K.O. Stanfill, "Relating blow moldability to large amplitude oscillatory shear behavior," *Polymer Engineering and Science*, **34**(11), 888-893 (Mid-June, 1994).

[5] Stickel, J.J., J.S. Knutsen, and M.W. Liberatore, "Response of elastoviscoplastic materials to large amplitude oscillatoryshear flow in the parallel-plate and cylindrical-Couette geometries," *Journal of Rheology*, **57**(6), 1569-1596 (2013).

[6] Dealy, J.M., "Rheometers for Molten Plastics: A Practical Guide to Testing and Property Measurement," Van Nostrand Reinhold, New York (1982).

[7] Férec, J., M.C. Heuzey, G. Ausias and P.J. Carreau, "Rheological behavior of fiber-filled polymers under large amplitude oscillatory shear flow." *Journal of Non-Newtonian Fluid Mechanics*, **151**, 89–100 (2008).

[8] Mutel, A.T. and M.R. Kamal, "The effect of glass fibers on the rheological behavior of polypropylene melts between rotating parallel plates," *Polymer Composites*, **5**(1), 29-35 (1984).

[9] Mutel, A.T., "Rheological behavior and fiber orientation in simple flows of glass fiber filled polypropylene melts," PhD Thesis, Chemical Engineering Dept., McGill University, Montreal, Canada (1989).

[10] Ding, F., A.J. Giacomin, R.B. Bird and C.-B. Kweon, "Viscous dissipation with fluid inertia in oscillatory shear flow," *Journal of Non-Newtonian Fluid Mechanics*, **86**(3), 359-374 (September, 1999).

[11] Yosick, J.A., A.J. Giacomin, W.E. Stewart and Fan Ding, "Fluid inertia in large amplitude oscillatory shear," *Rheologica Acta*, **37**, 365-373 (1998).

[12] Yosick, J.A., "A kinetic network model for nonlinear flow behavior of molten plastics in both shear and extension", Masters Thesis, University of Wisconsin, Chemical Engineering Dept., Madison, WI (December, 1995).

[13] Giacomin, A.J. and J.M. Dealy, "Using large-amplitude oscillatory shear," Chapter 11, Collyer, A.A. and D.W. Clegg, eds., *Rheological Measurement*, 2nd ed., Kluwer Academic Publishers, Dordrecht, Netherlands, pp. 327-356 (1998).

[14] Giacomin, A.J. and J.M. Dealy, "Large-amplitude oscillatory shear," Chapter 4, Collyer, A.A., ed., *Techniques in Rheological Measurement*, Chapman and Hall, London & New York, pp. 99-121 (1993); Kluwer Academic Publishers, Dordrecht, pp. 99-121 (1993); Erratum: Corrections to Figs 11.5-11.7 are in Ref. [13] above.

[15] Giacomin, A.J., R.B. Bird, L.M. Johnson and A.W. Mix, "Large-amplitude oscillatory shear flow from the corotational Maxwell model," *Journal of Non-Newtonian Fluid Mechanics*, **166**(19-20), 1081–1099 (2011). Errata: In Eq. (66), "$20\mathrm{De}^2$" and "$10\mathrm{De}^2 - 50\mathrm{De}^4$" should be "$20\mathrm{De}$" and "$10\mathrm{De} - 50\mathrm{De}^3$"; after Eq. (119), "$(\zeta\alpha)$" should be "$\zeta(\alpha)$"; In Eq. (147), "$n-1$" should be "$n=1$"; In Eqs. (76) and (77), Ψ' and Ψ'' should be Ψ_1' and Ψ_1''; Throughout, Ψ_1^d, Ψ_1' and Ψ_1'' should be Ψ_1^d, Ψ_1' and Ψ_1''; In Eqs. (181) and (182), "1,21" should be "1,2"; see also Ref. (58) below.

[16] Bird, R.B., R.C. Armstrong, and O. Hassager, *Dynamics of polymeric liquids*, Vol. 1, 2nd ed., Wiley, New York (1987). Erratum: In Eq. (10.1-10c), $\mathscr{R}e(\tau_{\theta z})$ should be $\tau_{\theta z}$.

[17] MacSporran, W.C. and R.P. Spiers, "The dynamic performance of the Weissenberg rheogoniometer II. Large amplitude oscillatory shearing - fundamental response," *Rheologica Acta*, **21**, 193-200 (1982).

[18] Fahimi, A., C.P. Broedersz, T.H.S. van Kempen, D. Florea, G.W.M. Peters and H.M. Wyss, "A new approach for calculating the true stress response from large amplitude oscillatory shear (LAOS) measurements using parallel plates," *Rheologica Acta*, **53**, 75–83 (2014).

[19] Phan-Thien, N., M. Newberry and R.I. Tanner, "Nonlinear oscillatory flow of a soft solid-like viscoelastic material," *Journal of Non-Newtonian Fluid Mechanics*, **92**(1), 67–80 (2000).

[20] Ng, T.S.K., G.H. McKinley, and R.H. Ewoldt, "Large amplitude oscillatory shear flow of gluten dough; a model power-law gel: Supplemental Information: Parallel plate correction with large amplitude oscillatory shear," *Journal of Rheology*, **55**(3), 627-654 (2011), pp. 1-7/7.

[21] Ng , T.S.K. and G.H. McKinley, "Large amplitude oscillatory shear flow of gluten dough: A model power-law gel," *Journal of Rheology*, **55**(3), 627-654 (2011).

[22] Whitaker, S., and R.L. Pigford, "An approach to numerical differentiation of experimental data," *Industrial & Engineering Chemistry*, **52**, 185-187 (1960).

[23] Adrian, D.W., "The quasi-periodic nature of wall slip for molten plastics in large amplitude oscillatory shear," Masters Thesis, Texas A&M University, Mechanical Engineering Dept., College Station, TX (March, 1992).

[24] Adrian, D.W. and A.J. Giacomin, "The quasi-periodic nature of a polyurethane melt in oscillatory shear," *Journal of Rheology*, **36**(7), 1227-1243 (October, 1992).

[25] MacSporran, W.C. and R.P. Spiers, "The dynamic performance of the Weissenberg rheogoniometer III. Large amplitude oscillatory shearing - harmonic analysis," *Rheologica Acta*, **23**, 90-96 (1984).

[26] Wilhelm, M., P. Reinheimer and M. Ortseifer, "High sensitivity Fourier-transform rheology," *Rheologica Acta*, **38**, 349-356 (1999).

[27] Wilhelm, M., K. Reinheimer and J. Kübel, "Optimizing the sensitivity of FT-rheology to quantify and differentiate for the first time the nonlinear mechanical response of dispersed beer foams of light and dark beer," *Zeitschrift für physikalische Chemie*, **226**, 547-567 (2012).

[28] Pearson, D.S. and W.E. Rochefort, "Behavior of concentrated polystyrene solutions in large-amplitude oscillating shear fields," *Journal of Polymer Science: Polymer Physics Edition*, **20**, 83 (1982); Errata: on p. 95, $e^{i\omega s}$ should be $e^{-i\omega s}$ in Eq. (A2); after Eq. (A10), α should be $\sqrt{\omega\tau_d/2}$; and in Eq. (A11), $\cos x$ should be $\cosh x$; in Eq. (A7), $\sqrt{2\alpha}$ should be $\sqrt{2}\alpha$.

[29] Powell, R.L. and W.H. Schwarz, "Geometrical effects in the measurements of mechanical properties in parallel superposed flows," *Journal of Polymer Science: Polymer Physics Edition*, **17**, 969- 985 (1979).

[30] Powell, R.L. and W.H. Schwarz, "Nonlinear dynamic viscoelasticity," *Journal of Rheology* **23**(3), 323- 352 (1979).

[31] Spiers, R.P., PhD Thesis, University of Bradford, Bradford, United Kingdom (1977).

[32] Wilhelm, M., D. Maring and H.-W. Spiess, "Fourier-transform rheology," *Rheologica Acta*, **37**(4), 399-405 (1998).

[33] Wilhelm, M., "Fourier-transform rheology," Thesis for the German *Habilitation*, Max-Planck-Institut für Polymerforschung, Mainz, Germany (December 2000).

[34] Wilhelm, M., "Fourier-transform rheology," *Macromolecular Materials and Engineering*, **287** (2), 83-105 (2002).

[35] Ahirwal, D., S. Filipe , G. Schlatter , M. Wilhelm, "Large amplitude oscillatory shear and uniaxial extensional rheology of blends from linear and long-chain branched polyethylene and polypropylene," *Journal of Rheology*, **58**(3), 635-658 (2014).

[36] Hyun, K. and M. Wilhelm, "Establishing a new mechanical nonlinear coefficient Q from FT-rheology: first investigation of entangled linear and comb polymer model systems," *Macromolecules*, **42**, 411-422 (2009).

[37] Reinheimer, K. and M. Wilhelm, "April-Science: Charakterisierung von Hellen und Dunklen Bierschäumen durch Mechanische Obertonanalyse, FT-Rheologie, Bunsen-Magazin," *Zeitschrift für physikalische Chemie*, **15**(1), 52-55 (February, 2013).

[38] Dötsch, T., M. Pollard and M. Wilhelm, "Kinetics of isothermal crystallization in isotactic polypropylene monitored with rheology and Fourier-transform rheology," *Journal of Physics: Condensed Matter*, **15**, S923–S931 (2003).

[39] N. Dingenouts and M. Wilhelm, "New developments for the mechanical characterization of materials," *Korea-Australia Rheology Journal*, **22**(4), 317-330 (December, 2010).

[40] Wagner, M.H., V.H. Rolón-Garrido, K. Hyun and M. Wilhelm, "Analysis of medium amplitude oscillatory shear data of entangled linear and model comb polymers," *Journal of Rheology*, **55**(3), 495-516 (2011).

[41] Davis, W.M. and C.W. Macosko, "Nonlinear dynamic mechanical moduli for polycarbonate and PMMA," *Journal of Rheology*, **22**, 53-71 (1978).

[42] Fan, X.-J. and R.B. Bird, "A kinetic theory for polymer melts VI. Calculation of additional material functions," *Journal of Non-Newtonian Fluid Mechanics*, **15**, 341-373 (1984).

[43] Bird, R.B. W.E. Stewart and E.N. Lightfoot, *Transport Phenomena*, Revised 2nd ed., Wiley, New York (2007).

[44] Bird, R.B., R.C. Armstrong and O. Hassager, *Dynamics of Polymeric Liquids*, Vol. 1, 1st ed., Wiley, New York (1977).

[45] Baek, H.M. (백형민) and A.J. Giacomin, "Corotating or codeforming models for thermoforming," *Journal of Advanced Engineering* (先進工程學刊), **8**(2), 41-54 (April, 2013).

[46] Baek, H.M., "Corotating or codeforming rheological models for thermoforming," Masters Thesis, University of Wisconsin, Mechanical Engineering Dept., Madison, WI (February, 2013).

[47] Johnson, L.M., A.J. Giacomin and A.W. Mix, "Viscoelasticity in thermoforming," *Journal of Polymer Engineering*, **32**(4-5), 245–258 (June 2012).

[48] Johnson, L.M., "Viscoelasticity in thermoforming," Masters Thesis, University of Wisconsin, Materials Science Program, Madison, WI (May, 2011).

[49] Baek, H.M. and A.J. Giacomin, "Corotating or codeforming models for thermoforming: free forming," Proceedings, Paper No. MSEC2013-1114, *Advances in forming*, Joint Meeting: ASME 8th International Manufacturing Science and Engineering Conference (MSEC 2013) and SME North American Manufacturing Research Conference (NAMRC41), Madison, WI (June 10-14, 2013), pp. V001T01A066; 9 pages.

[50] Middleman, S., *Fundamentals of Polymer Processing*, McGraw-Hill, New York (1977).

[51] Mertz, A.M., A.W. Mix, H.M. Baek and A.J. Giacomin, "Understanding melt index and ASTM D1238," *Journal of Testing and Evaluation*, **41**(1), 1-13 (2013).

[52] Mertz, A.M., "Understanding melt flow index and ASTM D1238," Masters Thesis, University of Wisconsin, Mechanical Engineering Dept., Madison, WI (July, 2012).

[53] Dhori, P.K., A.J. Giacomin and J.C. Slattery, "Common line motion II: Sliding plate rheometry," *Journal of Non-Newtonian Fluid Mechanics*, **71**(3), 215-229 (August, 1997).

[54] Adrian, D.W. and A.J. Giacomin, "The Transition to quasi-periodicity for molten plastics in large amplitude oscillatory shear," *Journal of Engineering Materials and Technology*, **116**, 446-450 (1994).

[55] Jeyaseelan, R.S., A.J. Giacomin, P.K. Dhori and J.C. Slattery, "Polymer melt instability in large amplitude oscillatory shear between sliding plates," S.P.E. Tech. Paper, **XXXXI**, Proc. 53rd Annual Tech. Conf. & Exhib., Society of Plastics Engineers, Boston, MA (May 7-11, 1995), pp. 1106-1110.

[56] Slattery, J.C. and A.J. Giacomin, "Method of extruding plastics," United States Patent No. 5,637,268 (June 10, 1997).

[57] Jeyaseelan, R.S., A.J. Giacomin and J.C. Slattery, "The effect of degassing on wall slip of LLDPE in large amplitude oscillatory shear," S.P.E. Tech. Paper, **XXXIX**, Vol. 3, Proc. 51st Annual Tech. Conf. & Exhib., Society of Plastics Engineers, New Orleans, LA (May 9-13, 1993), pp. 2611-2613.

[58] Giacomin, A. J., R.B. Bird, L.M. Johnson, and A.W. Mix, 'Corrigenda: "Large-amplitude oscillatory shear flow from the corotational Maxwell model," [Journal of Non-Newtonian Fluid Mechanics, **166**, 1081 (2011)],' *Journal of Non-Newtonian Fluid Mechanics*, **187-188**, 48 (2012).

[59] Merger, D. and M. Wilhelm, "Intrinsic nonlinearity from LAOStrain-experiments on various strain- and stress-controlled rheometers: a quantitative comparison," *Rheologica Acta*, DOI 10.1007/s00397-014-0781-3, published online (July 3, 2014).

[60] Mark, J.E., ed., *Physical properties of polymers handbook*, 2nd ed., Springer, New York (2007).

[61] "Standard test method for assignment of the glass transition temperatures by differential scanning calorimetry," ASTM E 1356-03, ASTM International, West Conshohocken, PA (2003).

[62] "Standard test method for plastics: dynamic mechanical properties melt rheology," ASTM D 4440-07, ASTM International, West Conshohocken, PA (2007).

[63] "Plastics — Determination of dynamic mechanical properties — Part 10: Complex shear viscosity using a parallel plate oscillatory rheometer," ISO 6721-10:1999(E), 2nd ed., ISO (December 15, 1999).

[64] Schweizer, Th., "Comparing cone-partitioned plate and cone-standard plate shear rheometry of a polystyrene melt," *Journal of Rheology*, **47**, 1071 (2003).

[65] Schweizer , T., "Measurement of the first and second normal stress differences in a polystyrene melt with a cone and partitioned plate tool," *Rheologica Acta*, **41**, 337-344 (2002).

[66] Schweizer, T., J. van Meerveld, and H.C. Öttinger, "Nonlinear shear rheology of polystyrene melt with narrow molecular weight distribution-Experiment and theory," *Journal of Rheology*, **48**, 1345-1363 (2004).

[67] Schweizer , T., "A quick guide to better viscosity measurements of highly viscous fluids," *Applied Rheology*, **14**(4), 197-201 (2004).

[68] Snijkers, F. and D. Vlassopoulos, "Cone-partitioned-plate geometry for the ARES rheometer with temperature control," *Journal of Rheology*, **55**, 1167-1186 (2011).

[69] Giacomin, A.J. and Dealy, J.M. "A new rheometer for molten plastics," S.P.E. Tech. Papers, **XXXII**, Proc. 44th Annual Tech. Conf., Society of Plastics Engineers, Boston, MA (May, 1986), pp. 711-714.

[70] Giacomin, A.J., "A sliding plate melt rheometer incorporating a shear stress transducer," Dept. Chemical Engineering, McGill University, Montreal, Canada (1987).

[71] Giacomin, A.J., T. Samurkas, and J.M. Dealy, "A novel sliding plate rheometer for molten plastics," *Polymer Engineering and Science*, **29**(8), 499-504 (April, 1989).

[72] Kolitawong, C., A.J. Giacomin and L.M. Johnson, "Shear stress transduction," Cover Article, *Review of Scientific Instruments*, **81**(2), 021301, 1-20 (2010).

[73] Kolitawong, C., A.J. Giacomin and L.M. Johnson, "Assumed periodicity and dynamic shear stress transduction in rheometry," *Journal of Rheology*, **54**(4), 835-858 (July/August, 2010).

[74] Kolitawong, C., "Local shear stress transduction in sliding plate rheometry," PhD Thesis, University of Wisconsin, Mechanical Engineering Dept., University of Wisconsin, Madison, WI (December, 2002).

[75] van Dusschoten, D. and M. Wilhelm, "Increased torque transducer sensitivity via oversampling," *Rheologica Acta*, **40**, 395-399 (2001).

[76] Wilhelm, M., "Methods and apparatus for detecting rheological properties of a material," United States Patent No. 6,357,281 B1 (March 19, 2002).

[77] Cox, W.P and E.H. Merz "Correlation of dynamic and steady flow viscosities," *Journal of Polymer Science,* **XXVIII**(118), 619-622 (1958).

[78] Macosko, C.W., "Rheology: Principles, measurements, and applications," Wiley-VCH, New York (1994).

[79] Brunn, P.O. and J. Vorwerk, "Determination of the steady-state shear viscosity from measurements of the apparent viscosity for some common types of viscometers," *Rheologica Acta*, **32**, 380-397 (1993).

[80] Giesekus, H. and G. Lanqer, "Die Bestimmung der wahren Fiießkurven nicht-newtonscher Flüssigkeiten und plastischer Stoffe mit der Methode der repräsentativen Viskosität," *Rheologica Acta*, **16**, 1-22 (1977).

[81] Shaw, M.T. and Z.Z. Liu **,** "Single-point determination of nonlinear rheological data from parallel-plate torsional flow," *Applied Rheology*, **16**(2) 70– 79 (2006).